

IOSUD – „DUNAREA DE JOS” UNIVERSITY OF GALATI

Doctoral School of Mechanical and Industrial Engineering



PhD THESIS

Abstract

MATHEMATICAL MODELS AND COMPUTER APPLICATION FOR BIOMECHANICAL ANALYSIS

PhD student,

Iuliana-Monica NOVETSCHI

Scientific coordinator,

Prof. dr. eng. ec. Elena MEREUTA

Series I6: Mechanical Engineering No. 77

GALATI

2024

IOSUD – „DUNAREA DE JOS” UNIVERSITY OF GALATI

Doctoral School of Mechanical and Industrial Engineering



PhD THESIS

Abstract

MATHEMATICAL MODELS AND COMPUTER APPLICATION FOR BIOMECHANICAL ANALYSIS

PhD student,

Iuliana-Monica NOVETSCHI

**Chairman of the
doctoral
committee
Scientific
coordinator,**

Prof. dr. eng. Eugen-Victor-Cristian RUSU

Prof. dr. eng. Elena MEREUTA

**Scientific
Rapporteurs**

1. Prof. dr. eng. Daniel CONDURACHE – "Gheorghe Asachi" Technical University of Iasi
2. Prof. dr. eng. Sorin-Ştefan BIRIŞ – National University of Science and Technology Politehnica of Bucharest
3. Prof. dr. eng. Mihaela BUCIUMEANU – „Dunarea de Jos” University of Galati

Series I6: Mechanical Engineering No. 77

GALATI

2024

The series of doctoral theses publicly defended in UDJG starting from October 1, 2013, are:

The fundamental field of ENGINEERING SCIENCES

Series I 1: Biotechnologies
Series I 2: Computers and Information Technology
Series I 3: Electrical Engineering
Series I 4: Industrial Engineering
Series I 5: Materials Engineering
Series I 6: Mechanical Engineering
Series I 7: Food Engineering
Series I 8: Systems Engineering
Series I 9: Engineering and Management in Agriculture and Rural Development

The fundamental field of SOCIAL SCIENCES

Series E 1: Economy
Series E 2: Management
Series E 3: Marketing
SSEF Series: Science of Sport and Physical Education
SJ Series: Straight
The fundamental field HUMANITIES
Series U 1: Philology- English
Series U 2: Philology - Romanian
Series U 3: History
Series U 4: Philology - French

The fundamental field of MATHEMATICS AND NATURAL SCIENCES

Series C: Chemistry

The fundamental field of BIOMEDICAL SCIENCES

Series M: Medicine
Series F: Pharmacy

CUPRINS

CHAPTER 1	7
INTRODUCTION TO THE ANALYSIS OF THE BIOMECHANIC SYSTEM OF THE HUMAN BODY	7
1.1. The objectives pursued and the purpose of the doctoral thesis	7
1.2. The architecture of the biomechanical system	7
1.3. Types of movements and their kinematic characterization	7
1.4. Principles of modelling biomechanical systems.....	9
1.5. Parameterization of mathematical models.....	9
1.6. Estimation of anthropometric parameters.....	11
1.7. Models for biomechanical analysis of upper and lower limbs	12
1.8. Partial conclusions	12
CHAPTER 2	13
MATHEMATICAL MODEL FOR THE BIOMECHANIC ANALYSIS OF THE HEAD - NECK - SPINE SYSTEM.....	13
2.1 Introduction	13
2.2 Mathematical model for studying the biomechanics of the head-neck-spine subsystem	13
2.3 Mathematical model for studying the biomechanics of the head-neck-spine subsystem	14
2.4 Parameterization of the mathematical model for the study of the biomechanics of the head-neck-spine subsystem	15
2.5 Utility of the mathematical model of upper body biomechanics	16
2.6 Validation of the mathematical model of upper body biomechanics using neural networks	16
2.7 Partial conclusions	18
CHAPTER 3.....	19
KINEMATIC MODELLING OF HUMAN UPPER AND LOWER LIMBS	19
3.1. Introduction	19
3.2. Python	19
3.3. The Denavit-Hartenberg convention.....	20
3.4. Homogeneous transformations	21
3.4.1. Homogeneous translational transformation	21
3.4.2. Homogeneous rotation transformation.....	21
3.5. Kinematics of the human upper limb	22
3.5.1. Anatomical considerations.....	22
3.5.2. Kinematic model of the human upper limb.....	23
3.5.3. Mathematical modeling of the human upper limb.....	24
3.5.4. Pseudocode Algorithm for Positional Analysis of the Human Upper Limb.....	25
3.5.5. Results of the human upper limb positional analysis algorithm	27
3.6. The kinematic model of the human lower limb	28
3.6.1. Anatomical considerations.....	28

3.6.2. The kinematic model of the human lower limb	30
3.6.3. Mathematical modeling of the human lower limb	30
3.6.4. Pseudocode Algorithm for Positional Analysis of the Human Lower Limb.....	32
3.6.5. Results of the human lower limb positional analysis algorithm.....	33
3.7. Partial conclusions	35
CHAPTER 4.....	36
DYNAMIC MODELLING OF THE HUMAN UPPER LIMB.....	36
4.1. Introduction	36
4.2. Skeletal muscular system	37
4.2.1. The structure of skeletal muscle	37
4.2.2. Types of contractions specific to skeletal muscle.....	37
4.3. Finite element modeling of skeletal muscle	37
4.3.1. Parametric considerations of finite element simulation	37
4.3.2. Results obtained from finite element analysis	39
4.3.3. The conclusions of the finite element simulation.....	40
4.4. Mathematical model for skeletal muscle analysis	42
4.5. Phenomenological algorithm for the analysis of the biceps short end muscle	44
4.6. Pseudocode algorithm for phenomenological analysis of skeletal muscle.....	46
4.7. Conclusions	47
CHAPTER 5.....	49
GENERAL CONCLUSIONS OF THE MATHEMATICAL MODELING OF THE HUMAN MECHANICAL SYSTEM	49
5.1. General conclusions	49
5.2. Personal contributions.....	51
5.3. Future research directions	52
SELECTIVE BIBLIOGRAPHY	54

CHAPTER 1

INTRODUCTION TO THE ANALYSIS OF THE BIOMECHANIC SYSTEM OF THE HUMAN BODY

1.1. The objectives pursued and the purpose of the doctoral thesis

The main objective of the doctoral thesis is the development of theoretical informatics models of the movements generated by the human body based on which analyses and evaluations aimed at highlighting mechanical behaviour can be undertaken. Thus, the objectives pursued in the research and development of this doctoral thesis are:

- analysis of the current state of research regarding biomechanical analysis and especially biomechanical models;
- the identification and analytical substantiation of some biomechanical models developed by classical or current methods aimed at ensuring the analysis of the human locomotor system;
- the design of versatile biomechanical models based on anthropometric parameters so that the final response of the model can reach the precision and degree of parametric fidelity;
- substantiation of human kinematics and its validation with the help of mathematical and computer models;
- the use of virtual instrumentation for models intended for the dynamic behaviour of the human locomotor apparatus.

1.2. The architecture of the biomechanical system

Transposing the movements of the human body into the virtual environment involves the application of techniques and technologies specific to the biomechanical field. Biomechanics involves the study of movements with or without the action of the forces that generate these movements (Nenciu, 2012).

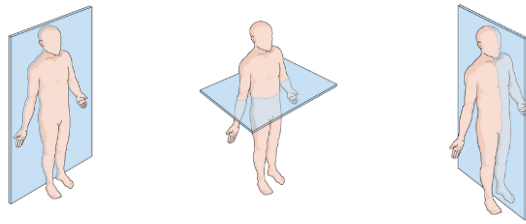
Important advances in the analysis of the movements of the human body have been registered in the last decade from the point of view of the techniques and technologies used.

1.3. Types of movements and their kinematic characterization

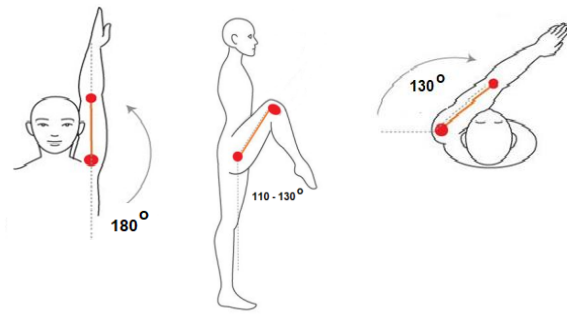
In biomechanics a mobile frame of reference typically originates at the body's center of gravity, moving with the body's motion.

For the reference systems to be unanimously accepted, the imaginary sectioning of the human body was made, in the orthostatic position, through which three main reference planes can be defined against which human movement is studied: the frontal plane, figure 1.1a; the transverse plan, figure 1.1b. and the sagittal plane, figure 1.1c.

Chapter 1. Introduction to the analysis of the biomechanic system of the human body



(a) (b) (c)
 Figure 1. 1. Anatomical planes (PAN): (a) frontal plane; (b) transverse plane; (c) sagittal plane



(a) (b) (c)
 Figure 1. 2. Elementary movements in normal anatomical planes. (a) in frontal plane - arm abduction; (b) in the sagittal plane – hip flexion; (c) internal arm rotation.

Depending on the defined planes and the movement axis, different movements are defined, figure 1.2: abduction and adduction movements; of flexion and extension; internal-external rotation.

The positional analysis of the kinematic elements is the starting point in the kinematic, kinetostatic and dynamic analysis in the field of biomechanics and involves the determination of the position vector (\vec{r}) in a two-dimensional or three-dimensional system of the position of the analyzed body, with the help of Cartesian coordinates (figure 1.4.) .

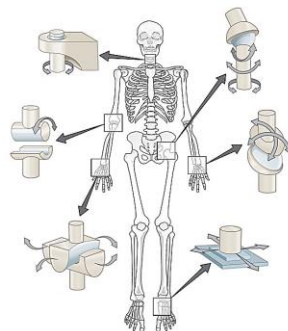


Figure 1. 3. Mechanical correspondence of anatomical joints

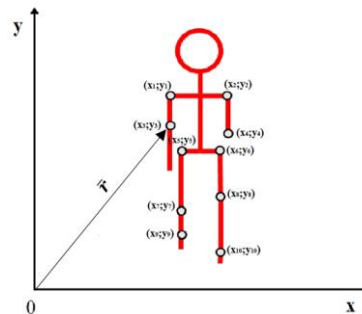
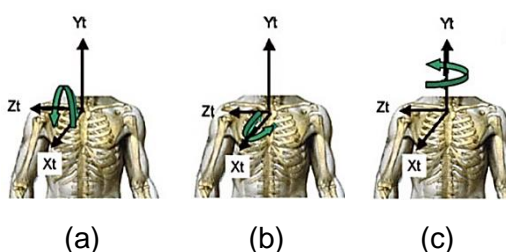
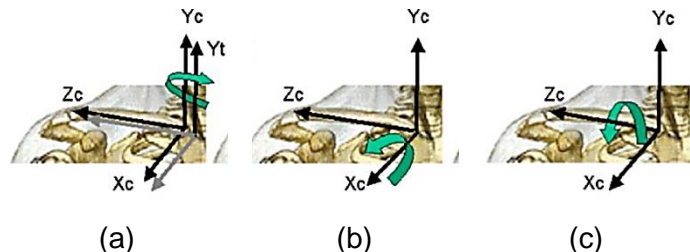


Figure 1. 4. Cartesian coordinates in the frontal plane.

At the level of the chest, the origin of the system is defined relative to the upper point of the sternum, against which the movements of flexion/extension (figure 1.5 a) and internal and external rotation (figure 1.5 b and 1.5 c) are related.



(a) (b) (c)
 Figure 1. 5. The relative coordinate systems of the chest to which its movement is related (a) flexion/extension (b) internal rotation (c) external rotation (Wu et al., 2005).



(a) (b) (c)
 Figure 1. 6. Relative coordinate systems of the clavicle relative to which its movement is reported (a) protraction/retraction; (b) elevation; (c) rotation (Wu et al., 2005)..

Chapter 1. Introduction to the analysis of the biomechanic system of the human body

In the case of the shoulder joint, the origin of the tri-orthogonal system is positioned in the centre of the glenohumeral rotation (Wu et al., 2005). Relative to the system in question, positive or negative elevations (figure 1.7 a and figure 1.7 b) and arm rotations (figure 1.7 c) are produced.

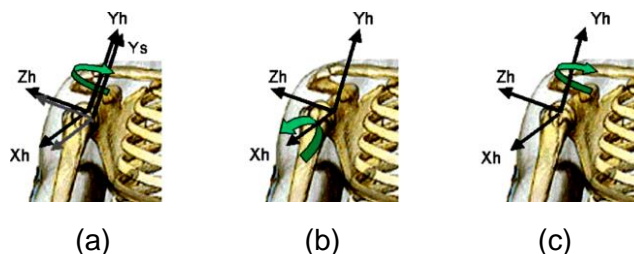


Figure 1. 7. Relative movements of the humerus relative to which its movement is related (a) plane of elevation (b) negative elevation (c) rotation (Wu et al., 2005).

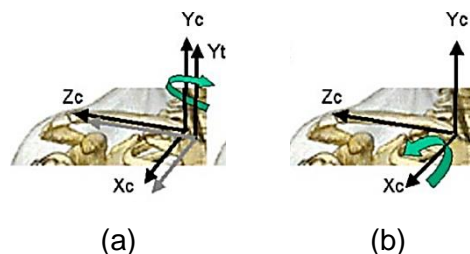


Figure 1. 8. Relative movements of the scapula: (a) protraction/retraction (b) rotation (Wu et al., 2005)

1.4. Principles of modelling biomechanical systems

Modeling of biomechanical systems or subsystems can be accomplished by using:

- a functional model that highlights components, phenomena and the interaction between them to result in the fundamental functions of the system;
- a theoretical model, on which theorems, formulas or principles are applied to describe the phenomenon, both qualitatively and quantitatively. Analytical modelling can take the form of mechanical models that approximate the real model as closely as possible. Such modelling calls for the conversion of anatomical subsystems into mechanical elements such as solid bodies, springs, and shock absorbers. The interaction of anatomical subsystems can be associated with forces, force couples, distributed loads, pressures, etc.

In biomechanical analysis, mathematical modelling makes use of a series of simplifying assumptions that are abandoned as the model improves. For example, in the modelling of the biomechanical systems of which the human skeleton is a part, it must be taken into account that the bone has a complex structure, and its mechanical and structural (geometric) properties determine the mechanical behaviour, giving it performance under loads. Due to its anisotropic and viscoelastic behaviour, bones behave and respond differently when loaded with different loads, directions and frequencies.

Muscle plays an important role in increasing bone strength, providing protection against mechanical stress and preserving or repairing bone tissue. As muscle and bone adapt and interact excellently, researchers must simultaneously measure muscle and bone when using these parameters in biomechanical modelling (Hart et al., 2017). The physical (real) model is described by a mathematical model that is developed in stages, as follows: writing the state equations; defining the link or transformation equations between the movements of the interacting subsystems; and establishing the physical laws applicable to the model. Due to the complexity of the analyzed phenomenon, establishing the equations of state can be extremely difficult.

1.5. Parameterization of mathematical models

In the development of the mathematical model, a line of compromise is generally adopted between the requirements related to a rigorous description of the process (complex equations) and the possibilities of numerical simulation. The model must contain a rigorous description of the system mechanisms. The model must have the minimum degree of

Chapter 1. Introduction to the analysis of the biomechanic system of the human body

complexity required by the purpose for which it was built. To develop a mathematical model, it is necessary to describe the interdependence between the variables, both in stationary and dynamic regimes.

Modelling the human body during a movement through a multi-body system allows a parameterization of its movement according to a series of angular parameters so that the overall movement can be described by the variation of these parameters as a function of time. The angular variation between the articulated elements is limited (constrained) anatomically by the type of articulation, by the insertions and origins of the muscles, but also by the shape of the bony condyles.

The occipito-atlantoid joint acts as a first-degree lever, with the fulcrum in the joint placed between the force given by the muscles of the neck and the resistance given by the weight of the head which tends to fall forward. This joint, together with the vertebrae in the cervical area, allows flexion movements with an amplitude of 90° , extension of 55° , lateral tilt of 35° and rotation of 140° (figure 1.14).

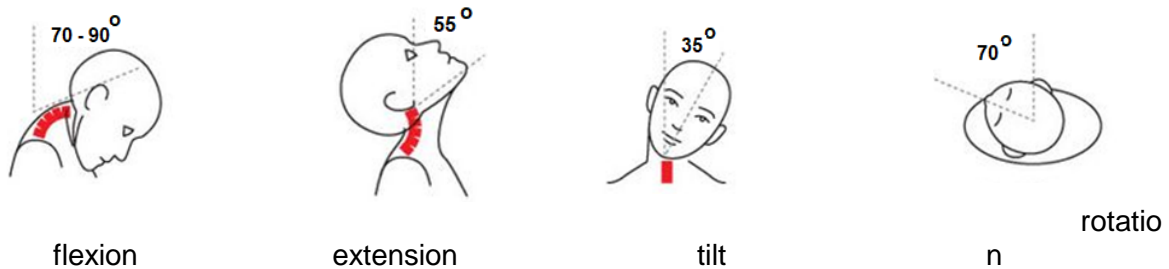


Figure 1.14. Ranges of angular variation of the head

The shoulder joint allows movements of the upper limb in the three anatomical planes: internal rotation (amplitude of 130°) and external rotation (amplitude of 45°), figure 1.15 a and b; abduction (amplitude of 180°) and adduction (amplitude of 45°), figure 1.15 c and d; flexion (amplitude of 180°) and extension (amplitude of 60°), figure 1.15 e and f.

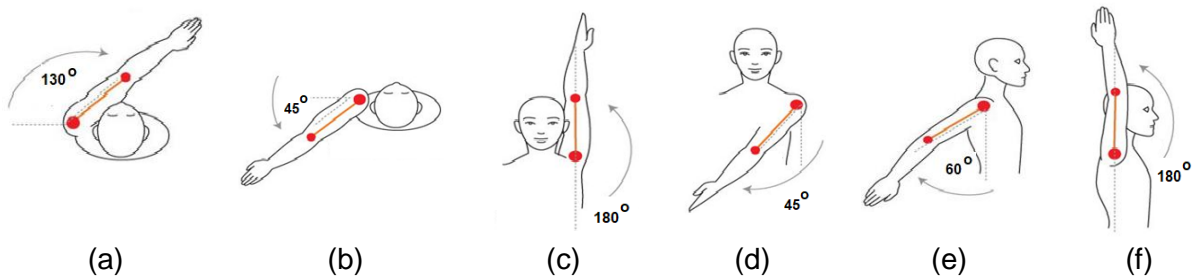


Figure 1.15. Angular amplitude of arm movements.

The movement of the upper limb is also determined by the amplitude of the angles of the elbow and wrist joints: the elbow identified as a cylindrical kinematic couple allows forearm flexion on the arm with an amplitude of 150° and an extension of 180° , figure 1.16; the wrist allows flexion-extension movements in a range of approximately 160° and deviation movements with respect to the two bones of the forearm by up to 50° , figure 1.7;

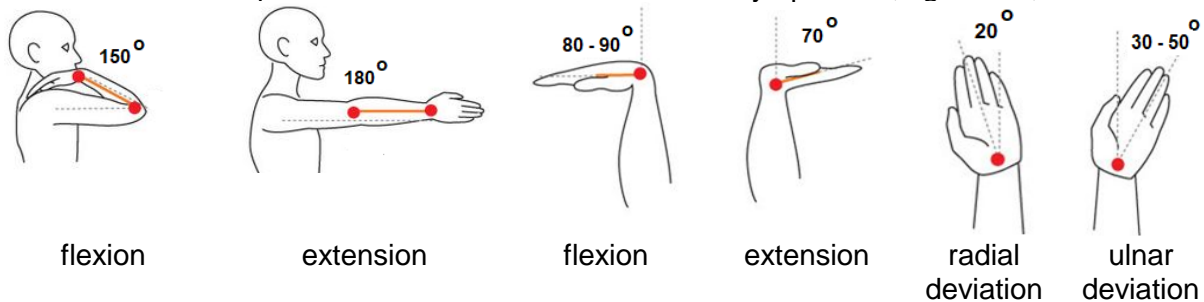


Figure 1.16. Angular amplitude of the elbow joint

Figure 1.17. Angular amplitude of the wrist joint.

1.6. Estimation of anthropometric parameters

Realistic modelling of biomechanical structures is based on the use of appropriate anthropometric parameters.

There are numerous studies published in the international specialized literature regarding the estimation of the anthropometric parameters of the human body segments. A chronological overview of these studies was developed in 1995 by Jørgen Bjørnstrup in the report "Estimation of Human Body Segment Parameters - Historical Background" (Bjørnstrup, 1995).

Several methods were used to estimate the anthropometric parameters of the human body segments of a certain individual (Robertson et al., 2004; Vaughan et al., 1992):

- measurements made on cadavers - require averaging the values obtained for large study groups, the results obtained are not specific to a certain individual (Robertson et al., 2004; Toth-Tascau & Stoia, 2011).
- mathematical modelling – requires the measurement of a finite number of parameters. Among the first studies of mathematical modelling of the inertial properties of the segments of the human body is the one carried out by Hanavan and Ernest in 1964 (Hanavan & Ernest, 1964). The methods created have been developed by other researchers to include more segments and more direct anthropometric measurements (Chen et al., 2021, 2021; Gismelseed et al., 2023; He et al., 2022; Pecolt et al., 2022; Peyer et al., 2015; Zhu et al., 2023);
- medical imaging techniques (X-rays, CT, MRI, etc.) – provide more accurate information, but have the disadvantage of exposure to certain radiation sources (Huang et al., 2022; Jiang et al., 2023; Kumar & Y, 2023; Ramasamy et al., 2023; Yousaf et al., 2023);
- kinematic measurements – do not provide accurate information and require a long time to perform the measurements and process the data [Robertson et al., 2004].

In 1975 Hatze, in the work "The complete optimization of a human motion", developed the oscillation technique by which he determines the mass and moments of inertia of the limb segments and the damping coefficient in the joints. The technique cannot be used for trunk segments because it requires a part of the body to be involved in an oscillating motion with an apparatus containing a spring (Hatzé, 1976). The muscles must be relaxed so as not to influence the damped oscillations of the spring-limb system (Robertson et al., 2004).

Figure 1.18 shows a model of the human body represented in the form of zonal segments. This model was used in the studies carried out within the Digital Human Research Center project, for the development of databases (Human Body Properties Database) relating to subjects from Japan, the U.S.A. and Europe [DHRC, 2009]:

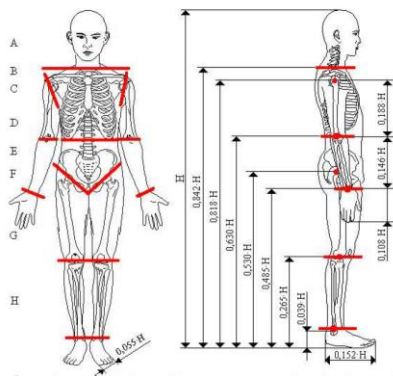


Figure 1. 18. Segmentation of the human body into the most important areas and estimation of dimensions according to height.

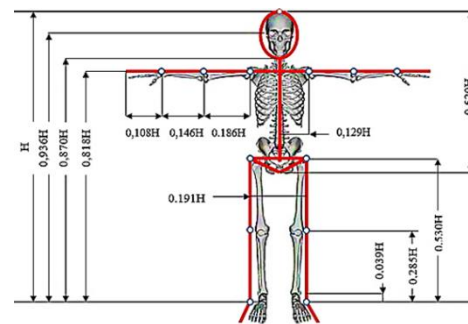


Figure 1. 19. General scheme for calculating the lengths of anatomical segments [Miller D.I., 1973].

Chapter 1. Introduction to the analysis of the biomechanic system of the human body

The masses of some segments of the human body can be determined in relation to the total body mass, using data from the specialized literature [Hall S.J., 1995; Miller, D.I., 1973]

1.7. Models for biomechanical analysis of upper and lower limbs

The wide mobility of the human body leads to the need to model the osteoarticular system as a mechanism with a large number of degrees of freedom.

Thus, a dynamic model considers the human upper limb as a mechanical system with 5 degrees of freedom (Naaji, 2008), another with 7 degrees of freedom (Pennestri et al., 2007), with 7 degrees of freedom and 17 muscles that generate real-time estimates of the neural discharge patterns of the muscle spindle and the Golgi tendon organ (Williams & Constandinou, 2014) or a matrix approach to the mathematical model of the upper limb considered as a mechanism with spherical joints with n degrees of freedom (Gillawat, 2022)

Using OpenSim software (Lai et al., 2021), a musculoskeletal model of the upper limbs widely used in research was validated. Muscle activation results from its static optimization were evaluated against real-world data.

In (Bahadori & Wainwright, 2020) for the biomechanical assessment of the lower limbs in healthy individuals, separate protocols were developed for gait analysis and muscle strength testing. The estimation of kinematic and kinetic parameters of healthy and pathological gait can be performed using a complete musculoskeletal model, obtained by modelling 14 bones, 88 musculotendinous Hill segments, ten ligament segments for each knee and six joints for each lower limb (Cardona & Garcia Cena, 2019).

The geometric model with 7 degrees of freedom (DOF) (3 DOF in the hip joint, 2 DOF in the knee joint and 2 DOF in the ankle joint) proposed by (Rusu et al., 2014) develops and validates the mathematical model of human lower limbs based on the Denavit-Hartenberg (D-H) robotics convention. Designing a robot with six rotational degrees of freedom, including two leg joints, with hip support is another example of modelling and simulating a lower limb exoskeleton. The three-dimensional structural model was built in SolidWorks, and its mathematical model was made using the methodology of W. Khalil and E. Dombre (Jaimes et al., 2021).

1.8. Partial conclusions

In this chapter I made an introduction to the analysis of the biomechanical system of the human body, highlighting the objectives of the doctoral thesis and the architecture of the biomechanical system. The thesis aims to develop theoretical informatics models of human body movements for accurate analyses. The types of movements and reference systems used in biomechanics are also discussed. This information is essential for the further understanding of the biomechanical behaviour of the human body.

The principles of modelling biomechanical systems highlight the various techniques and models used in this field of research, using functional models, which highlight components and interactions to result in system functions, or theoretical models, based on which phenomena are described, both qualitatively and quantitatively.

CHAPTER 2

MATHEMATICAL MODEL FOR THE BIOMECHANIC ANALYSIS OF THE HEAD - NECK - SPINE SYSTEM

2.1 Introduction

Systematic classification of cervical spine models revealed the following trends: multi-body modelling for simulating impact situations, inverse dynamics, optimization, and the Hill muscle model. To these are added the models that propose to validate the results through comparisons with data from the literature, most of them not being able to confirm the similarity with the real model (Alizadeh et al., 2020). Mathematical modelling was also used to determine the kinematics of the upper limb, using rotation matrices and homogeneous transformations (M. M. Novetschi et al., 2023), mathematical models based on finite element analysis of the neck and head-neck biomechanical subsystem and model validation with data collected from subjects (Meyer et al., 2021), mathematical models based on detailed three-dimensional models and MBS (Multibody simulation) for simulating the dynamic behaviour of the head-neck subsystem during accidents (De Jager et al., 1996).

2.2 Mathematical model for studying the biomechanics of the head-neck-spine subsystem

The proposed model starts from the equation of movement of the human head in a biomechanical system with three degrees of freedom using Lagrange equations of the second kind. The biomechanical system is made up of 3 anatomical elements: the head, the cervical area and the rest of the spine (considered as a single element consisting of the thoracic area, the lumbar area, the sacral area and the coccygeal area) (figure 2.1), and the main purpose of this model was to obtain the differential equations of motion in matrix-analytical form (Amortila et al., 2021).

Thus, the movement of the biomechanical system was analyzed in the sagittal plane considering the subsystem as an inverted triple pendulum, and the joints as cylindroids. The different interpretation of the origin and insertions of the muscles (as the main generator of movement) for some biomechanical models associated with the human body causes different interpretations of the phenomena.

The masses and the position of the centre of gravity were estimated for the three elements – head, neck and spine – starting from the total mass and the dimensions of the segments (through anthropometric measurements) [[https://mec.tuiasi.ro/diverse/Indrumar_lucrari_aplicative-Biomecanica .pdf](https://mec.tuiasi.ro/diverse/Indrumar_lucrari_aplicative-Biomecanica.pdf)].

The mechanical model used for the analysis of this biomechanical system is a triple-inverted physical pendulum consisting of 2 articulated bars (the spine and the neck) and a sphere (the head), (figure 2.2.).

2.3 Mathematical model for studying the biomechanics of the head-neck-spine subsystem

The proposed model starts from the equation of movement of the human head in a biomechanical system with three degrees of freedom using Lagrange equations of the second kind. The biomechanical system is made up of 3 anatomical elements: the head, the cervical area and the rest of the spine (considered as a single element consisting of the thoracic area, the lumbar area, the sacral area and the coccygeal area) (figure 2.1), and the main purpose of this model was to obtain the differential equations of motion in matrix-analytical form (Amortila et al., 2021).

Thus, the movement of the biomechanical system was analyzed in the sagittal plane considering the subsystem as an inverted triple pendulum, and the joints as cylindroids. The different interpretation of the origin and insertions of the muscles (as the main generator of movement) for some biomechanical models associated with the human body causes different interpretations of the phenomena.

The masses and the position of the centre of gravity were estimated for the three elements – head, neck and spine – starting from the total mass and the dimensions of the segments (through anthropometric measurements) [https://mec.tuiasi.ro/diverse/Indrumar_lucrari_aplicative-Biomecanica .pdf].

The mechanical model used for the analysis of this biomechanical system is a triple-inverted physical pendulum consisting of 2 articulated bars (the spine and the neck) and a sphere (the head), (figure 2.2.).

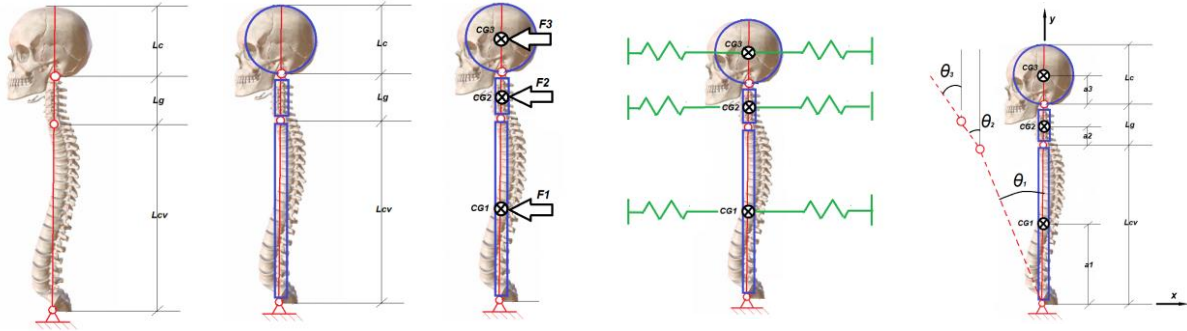


Figure 2. 1 Head, neck, spine biomechanical system

Figure 2. 2 Triple inverted pendulum

Figure 2. 3 Mechanical model with disruptive forces

The proposed physical model presents 3 degrees of freedom, and the disturbing forces F_1 , F_2 , F_3 , act in the centers of gravity of the elements and change the orthostatic position of the body (figure 2.3).

The potential energy of the analyzed subsystem is composed of the potential energy of each element and the potential energies of the limiting springs:

$$E_p = E_{p1} + E_{p2} + E_{p3} + 2E_{pa1} + 2E_{pa2} + 2E_{pa3} \quad (2.23)$$

$$E_p = \frac{1}{2} [m_1 \cdot g \cdot a_1 + m_2 \cdot g \cdot L_{cv} + m_3 \cdot g \cdot L_{cv} + 2 \cdot k_1 \cdot a_1^2 + 2 \cdot k_2 \cdot L_{cv}^2 + 4 \cdot k_3 \cdot L_{cv}^2] \cdot \theta_1^2 + \frac{1}{2} [m_2 \cdot g \cdot a_2 + m_3 \cdot g \cdot L_g + 2 \cdot k_2 \cdot a_2^2 + 2 \cdot k_3 \cdot L_g^2] \cdot \theta_2^2 + \frac{1}{2} [m_3 \cdot g \cdot a_3 + 2 \cdot k_3 \cdot a_3^2] \cdot \theta_3^2 + \frac{1}{2} [4 \cdot k_2 \cdot a_2 \cdot L_{cv} + 4 \cdot k_3 \cdot L_g \cdot L_{cv}] \cdot \theta_1 \theta_2 + \frac{1}{2} [4 \cdot k_3 \cdot a_3 \cdot L_g] \cdot \theta_2 \theta_3 + \frac{1}{2} [4 \cdot k_3 \cdot a_3 \cdot L_{cv}] \cdot \theta_1 \theta_3 + \frac{1}{2} [4 \cdot k_1 \cdot x_{f1} \cdot a_1 + 4 \cdot k_2 \cdot L_{cv} + 4 \cdot k_3 \cdot x_{f3} \cdot L_{cv}] \cdot \theta_1 + \frac{1}{2} [4 \cdot k_2 \cdot x_{f2} \cdot a_2 + 4 \cdot k_3 \cdot x_{f3} \cdot L_g] \cdot \theta_2 + \frac{1}{2} [4 \cdot k_3 \cdot x_{f3} \cdot a_3] \cdot \theta_3 \quad (2.34)$$

The equation that describes the potential energy of the system according to the three generalized coordinates, θ_1 , θ_2 , θ_3 , is derived in turn. By identifying the terms in the general

Chapter 2. Mathematical model for the biomechanic analysis of the head - neck - spine system

form of the potential energy, the terms of the stiffness matrix are determined. The equation of motion for the analyzed model can be written in matrix form:

$$[M] \cdot \begin{Bmatrix} \ddot{\theta}_1 \\ \ddot{\theta}_2 \\ \ddot{\theta}_3 \end{Bmatrix} + [K] \cdot \begin{Bmatrix} \theta_1 \\ \theta_2 \\ \theta_3 \end{Bmatrix} = [F_{iP}] \quad (2.39)$$

By replacing the terms of the inertia matrix and those of the stiffness matrix, the system of equations that provide the expressions of the forces F1, F2 and F3 is obtained.

$$\left[\frac{m_1 \cdot L_{cv}^2}{3} + 2 \cdot m_2 \cdot L_{cv}^2 + m_3 \cdot L_{cv}^2 + m_2 \cdot L_{cv} \cdot a_2 \cdot \cos(\theta_2 - \theta_1) + m_3 \cdot L_{cv} \cdot L_g \cdot \cos(\theta_2 - \theta_1) + \frac{1}{2} \cdot m_3 \cdot L_{cv} \cdot a_3 \cdot \cos(\theta_3 - \theta_1) \right] \cdot \ddot{\theta}_1 + (m_1 \cdot g \cdot a_1 + m_2 \cdot g \cdot L_{cv} + m_3 \cdot g \cdot L_{cv} + 2 \cdot k_1 \cdot a_1^2 + 2 \cdot k_2 \cdot L_{cv}^2 + 4 \cdot k_3 \cdot L_{cv}^2 + 2 \cdot k_2 \cdot a_2 \cdot L_{cv} + 4 \cdot k_3 \cdot L_g \cdot L_{cv} + 2 \cdot k_3 \cdot a_3 \cdot L_{cv}) \cdot \theta_1 = F_1$$

$$\left[m_2 \cdot L_{cv} \cdot a_2 \cdot \cos(\theta_2 - \theta_1) + m_3 \cdot L_{cv} \cdot L_g \cdot \cos(\theta_2 - \theta_1) + \frac{m_2 \cdot L_g^2}{12} + m_2 a_2 + m_3 \cdot L_g^2 + \frac{1}{2} \cdot m_3 \cdot L_g \cdot a_3 \cdot \cos(\theta_3 - \theta_2) \right] \cdot \ddot{\theta}_2 + (2 \cdot k_2 \cdot a_2 \cdot L_{cv} + 4 \cdot k_3 \cdot L_g \cdot L_{cv} + m_2 \cdot g \cdot a_2 + m_3 \cdot g \cdot L_g + 2 \cdot k_2 \cdot a_2^2 + 2 \cdot k_3 \cdot L_g^2 + 2 \cdot k_3 \cdot a_3 \cdot L_g) \cdot \theta_2 = F_2$$

$$\left[\frac{1}{2} \cdot m_3 \cdot L_{cv} \cdot a_3 \cdot \cos(\theta_3 - \theta_1) + \frac{1}{2} \cdot m_3 \cdot L_g \cdot a_3 \cdot \cos(\theta_3 - \theta_2) + \frac{1}{5} m_3 \cdot L_C^2 + m_3 \cdot a_3^2 \right] \cdot \ddot{\theta}_3 + (2 \cdot k_3 \cdot a_3 \cdot L_{cv} + 2 \cdot k_3 \cdot a_3 \cdot L_g + m_3 \cdot g \cdot a_3 + 2 \cdot k_3 \cdot a_3^2) \cdot \theta_3 = F_3$$

2.4 Parameterization of the mathematical model for the study of the biomechanics of the head-neck-spine subsystem

Based on the developed mathematical model, a computer application was created in the C++ programming language to determine the values of the three disturbing forces responsible for removing the analyzed system from the equilibrium position. It is important to note that such a model should be validated using real-world data and observations to ensure relevance and similarity to real-world injury risk situations.

For the development of the IT application, it was considered that the maximum variation values of the three angles ($\theta_1, \theta_2, \theta_3$) are included in the range from 0° to 45°, and the movement that the system performs takes place in 1000 [ms].

For the proposed mathematical model, the anthropometric dimensions were used as input data and anthropometric measurements were made for 16 participants (table 2. 2). To solve the system of equations, a computer application was developed in C++ language, based on which the maximum and minimum values of the disturbing forces were determined for 16 subjects.

The graphs in Figure 2.4 show the linear characteristics of the muscle groups responsible for generating the movement of the analyzed subjects.

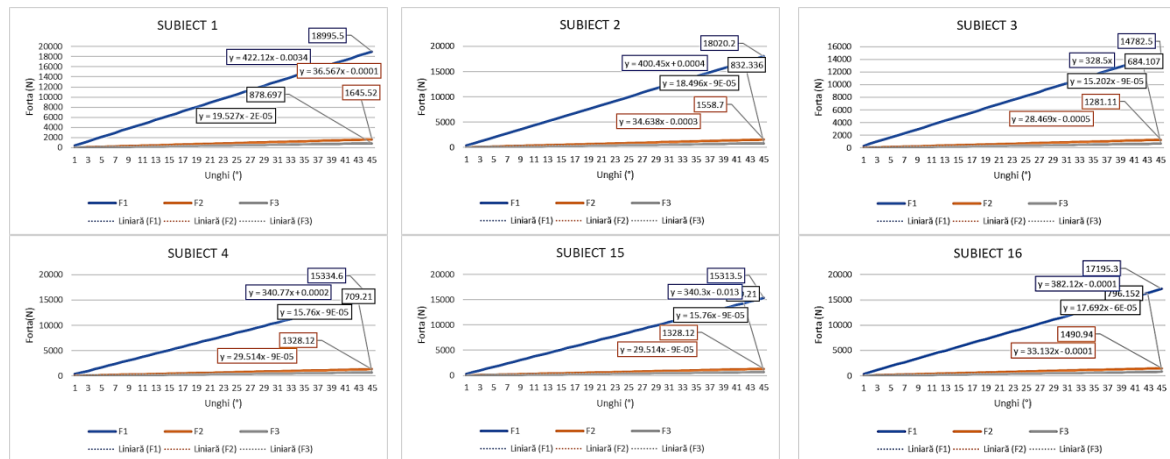


Figure 2. 4 Linear characteristics of muscle groups responsible for movement generation

2.5 Utility of the mathematical model of upper body biomechanics

The development of the mathematical model for the evaluation of muscle strength can be used in the evaluation and dimensioning of the passive safety systems (seat belts, airbags, materials for absorbing and dissipating energy) of a driver in the event of an accident.

There is no absolute maximum value for the impact force in a road accident that guarantees the safety of the passenger and the absence of injuries. This finding derives from the complexity of the variables that influence the consequences of an impact, including road conditions, the type of vehicles involved and other contingent factors.

The presented mathematical model can provide the forces that can be developed by the muscles, in response to the frontal impact of a motor vehicle. From the data presented following the parameterization of the model, it is found that the dynamic response of the upper body muscle groups for the 16 subjects is approximately 20 [KN]. In most cases, the frontal impact force exceeds the sum of the muscle group forces, which is why it is necessary to use additional passive safety measures to compensate for the difference in forces, i.e. between the impact force and the sum of the muscle group forces.

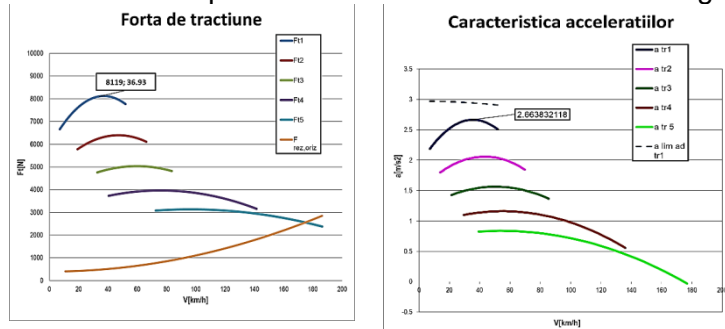


Figure 2. 5 Graph of vehicle driving force and acceleration for the 5 gears

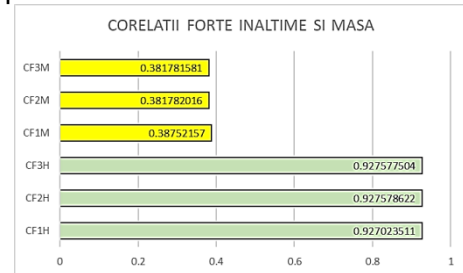


Figure 2. 6 Correlation between forces, mass and height

There is a correlation between a person's height and mass and muscle strength, but it is not always direct. We investigated the relationship between the physical dimensions of the subjects and the forces developed. We examined the correlation between subjects' height and mass and the forces generated. The three forces show a significant and positive correlation with subjects' mass (with a correlation coefficient greater than 0.9), while the correlation with subjects' height is more modest and generally less than 0.4.

2.6 Validation of the mathematical model of upper body biomechanics using neural networks

To validate a mathematical model using artificial neural networks (ANNs), it is essential to design a neural network architecture capable of learning the relationship between the input parameters of the biomechanical mathematical model - such as height and body mass - and its outputs, which represent the forces disruptors of the biomechanical elements. In the process of training the network, we used part of the data about the perturbing forces generated by the muscle groups responsible for the movement of the spine, neck and head, obtained through the mathematical model and a C++ application, while the rest of the data was reserved for network validation.

The neural network architecture was configured using the Easy NN application. After completing the training, we observed that the height of the subject was the most significant factor influencing the generation of muscle force, showing the highest sensitivity. Moreover, the muscle force values determined during the validation process were very close to those obtained by the mathematical model.

Chapter 2. Mathematical model for the biomechanic analysis of the head - neck - spine system

These findings suggest that the mathematical model is robust and that the neural network can be used to make accurate predictions regarding various subject sizes, even when their values do not correspond to the data range used to train the network.

After the model was trained we used the validation data set to evaluate its performance. The model was used to make predictions on the validation data and compare these predictions with the actual values provided by the mathematical model. After validation, a maximum error value of 2.633% and a minimum error value of 0.068% were obtained after 217 training cycles. The biggest errors were recorded in subjects with extreme height values, that is, at the ends of the range analyzed with the neural model. It can be stated that the neural network generalizes well with a maximum allowable error of 2.633% and that it was not over-trained (many training cycles) or under-trained (little input data).

The neural network graphically provides us with data on two key aspects in evaluating the performance and behaviour of the network: Importance (Importance) which indicates how much each input influences the final result of the network and Sensitivity (Sensitivity) refers to the degree to which changes in the inputs of the network or its parameters affect its output or prediction.

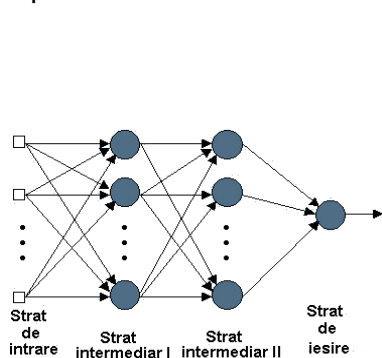


Figure 2. 7 General organization of the neural network architecture

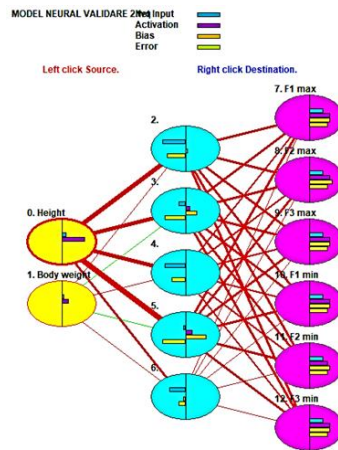


Figure 2. 9 Architecture of the neural model used to validate the mathematical model

We used the data generated by the mathematical model for 11 of the subjects to train the neural network. Training the network causes the synaptic weights to be adjusted so that the error between the provided output and the indicated value is within the prescribed limits.

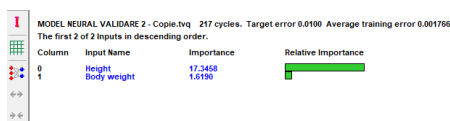


Figure 2. 12 Importance of input data on muscle force values

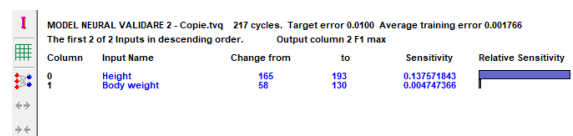


Figure 2. 13 Sensitivity of input data on muscle force values

Testing data with a neural network involves using the network to make predictions, data that is separate from the data set used for training. For testing and predictions, we used the data of 5 subjects that we did not use in training the network. The data were in the same format and covered different data than the training data (figure 2.14).

The maximum error of minimum forces obtained in neural model testing is less than the maximum error obtained in network training (2,571), for minimum forces, and the maximum error of maximum forces obtained in neural model testing is less than the maximum error obtained in network training (2.575) for maximum forces.

2.7 Partial conclusions

The advantages of mathematical modelling stand out, especially in the case of complex biomechanical systems when it is necessary to determine a series of parameters using non-invasive methods. Thus, the investigation of a particular subsystem is possible when actual experiments cannot be performed. At the same time, the use of the model allows iterating on various anthropometrics as many times as needed to be able to make a more accurate analysis. Also, by changing the parameters of the biomechanical system, the extreme values of the variables can be established, values that would correspond to anatomical limit positions. We can conclude that the model-based study is much more effective both qualitatively and economically (low costs, reduced time, etc.)

The head-neck-spine analytical model can be used when the angular variations of the studied anatomical elements (θ_1 , θ_2 , θ_3) can be determined. This is possible with a series of computer applications that use markers (Kinovea) or with the help of sensors that can determine angular displacements.

The developed model can determine the values of the forces responsible for the movement of the head, neck or trunk, but also the restorative forces responsible for returning the body to the orthostatic position.

Based on the developed mathematical model, a computer application was created in C++ programming language to determine the values of the three disturbing forces responsible for removing the analyzed system from the equilibrium position. Testing data with a neural network is a crucial step in the process of RNA model development and evaluation and plays an important role in generalizing the model for prediction. Easy NN software allows the advantage of exporting the trained neural model for use with other applications or to be integrated into other systems.

CHAPTER 3.

KINEMATIC MODELLING OF HUMAN UPPER AND LOWER LIMBS

3.1. Introduction

Bipedal walking is an autonomous activity considered as the main mode of locomotion for human beings. Due to the increase in the number of people with disabilities associated with the locomotor system, gait analysis is of particular relevance for purposes such as clinical diagnosis, sports medicine or biomechanics research for the design of locomotor assistive technologies (Islas et al., 2020; Kitade et al., 2020; Klöpfer-Krämer et al., 2020). In addition, interest in the development of humanoid robots is growing. The most well-known methods for the analysis of robot kinematics and implicitly of human kinematic chains are homogeneous transformations, the Denavit-Hartenberg convention, but also geometric methods.

The research methodology is presented in a summarized form in Figure 3.1. To achieve the goal, we went through three stages. The first stage refers to the input data associated with the mechanical system in question. Specifically, this data contains information about the length of the kinematic elements, the types of kinematic couples and the angular ranges. In the second stage, we determined the mathematical models for the direct kinematic analysis by the method of homogeneous transformations. It should be noted that both the homogeneous transformations and the Denavit-Hartenberg convention produce the same result. In this stage, the rotation matrices (R_i^{i-1}), the displacement vectors (d_i^{i-1}), but also the orientation of the tri orthogonal axis systems ($O_n x_n y_n z_n \rightarrow O_m x_m y_m z_m$) are deduced for each kinematic couple taken into account. In the third stage, I developed a script in the Python programming language that aims to determine the homogeneous transformation matrix.

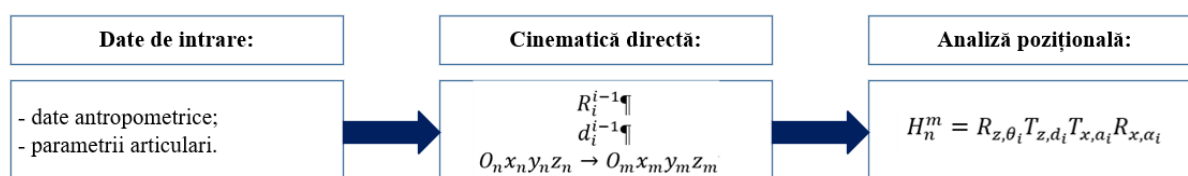


Figure 3. 1. Methodology for determining the position of the effector.

3.2. Python

I chose the Python language because it focuses on readability, consistency and software quality. These aspects differentiate it from other tools in the world of scripts and

software applications. Python code is designed to be readable and therefore reusable, but also easy to maintain (much more so than traditional scripting languages). The uniformity of Python code makes it easy to understand, even if it's written by someone else. In addition, Python contains support for advanced software reuse mechanisms such as object-oriented (OO) programming and functions (Lutz, 2003).

Python, compared to other programming languages, comes with a larger collection of portable and predefined functionality known as the standard library compared to other programming languages. Through integration mechanisms, Python scripts can easily communicate with other application systems. Such integrations allow Python to be used as a product customization and extension tool. Today, Python code can invoke C and C++ libraries, be called from C and C++ programs, integrate with Java and Microsoft .NET components, communicate through frameworks such as COM and Silverlight, interact with devices through serial ports, and networks with interfaces such as SOAP, XML-RPC and CORBA (Shein, 2015). An advantage of the Python programming language is that it allows database manipulation, statistical analysis, applying filters and graphical rendering of information in just a few lines of code, based on existing time-tested libraries.

3.3. The Denavit-Hartenberg convention

The Denavit-Hartenberg (D-H) convention is a convention commonly used in biomechanics, but also robotics for determining tri-orthogonal axis systems and kinematics. According to this convention, each homogeneous transformation H_n^m is represented as a product of four basic transformations. More precisely two rotations and two translations, equations 3.1 – 3.5.

In addition to the rotational movement, in the joints of the human body, some slides are modelled by plane-parallel movements or curvilinear translations. In the kinematic modelling of the human body or subassemblies (upper limbs, lower limbs, trunk, and others) the joints are considered fifth-class couples, the additional motions mentioned above not being essential for the description of the laws of motion.

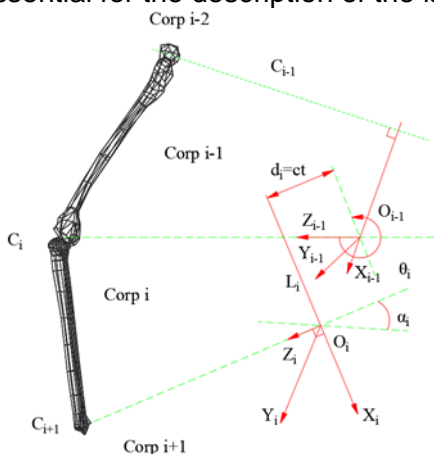


Figure 3. 2. Graphic representation of the Denavit-Hartenberg convention.

The movements in question are determined by the characteristic geometry of each joint, thus giving it the unique character of differentiation from another couple with a similar number of degrees of freedom. Thus, the particular role in the functionality of the anatomical system is highlighted. In other words, they are aspects of movement finesse that can be overlooked in kinematic modeling (K.-D. Nguyen et al., 2009).

According to the Denavit-Hartenberg convention, each coupling i has an associated joint variable q and is represented by a joint parameter θ (rotation angle) that varies around an axis or a displacement parameter along the coupling axis, d .

Transfer matrices can be expressed both by the Denavit-Hartenberg convention and by homogeneous transformations.

3.4. Homogeneous transformations

In the mathematical modeling of the human body, the importance of using homogeneous coordinates and the extended vector concept comes from the representation of equation 3.6, which is fundamental to the formulation of a systematic method of representing the motion of one segmental link relative to another.

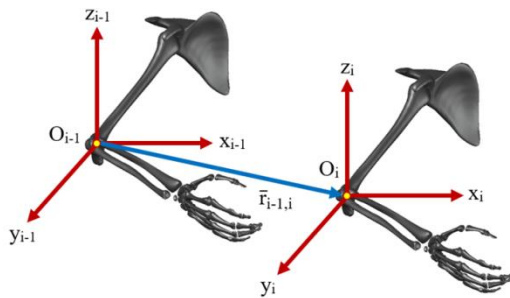
The matrix $H_{n \times m}$ is called the homogeneous transformation matrix and represents the coordinate transformation between positions m and n . In other words, applied to a rigid body causes a transformation, i.e. change of configuration (position and orientation) (Bajd et al., 2010; Martínez Martínez & Campa, 2021).

If we consider some point P on the surface of a body, then x, y and z are the coordinates in the Cartesian system. In a homogeneous coordinate system these coordinates are u, v, w , and n . The fourth coordinate is the dimensional norm equal to unity ($x = \frac{u}{n}; y = \frac{v}{n}; z = \frac{w}{n}$).

$$\begin{bmatrix} \bar{x}^m \\ 1 \end{bmatrix} = \begin{bmatrix} R_n^m & d_n^m \\ 0 & 1 \end{bmatrix} \begin{bmatrix} \bar{x}^n \\ 1 \end{bmatrix} \quad (3.6)$$

3.4.1. Homogeneous translational transformation

The translation of a body involves the multiplication of the general matrix with the homogeneous transformation matrix corresponding to the translation (Bajd et al., 2010). For example, the homogeneous translation transformation (figure 3.3) is expressed by:

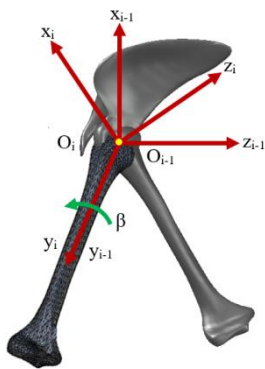


$$T \cdot G = \begin{bmatrix} 1 & 0 & 0 & \Delta x \\ 0 & 1 & 0 & \Delta y \\ 0 & 0 & 1 & \Delta z \\ 0 & 0 & 0 & 1 \end{bmatrix} \cdot \begin{bmatrix} n_x & o_x & a_x & p_x \\ n_y & o_y & a_y & p_y \\ n_z & o_z & a_z & p_z \\ 0 & 0 & 0 & 1 \end{bmatrix} = \begin{bmatrix} n_x & o_x & a_x & p_x + \Delta x \\ n_y & o_y & a_y & p_y + \Delta y \\ n_z & o_z & a_z & p_z + \Delta z \\ 0 & 0 & 0 & 1 \end{bmatrix} \quad (3.12)$$

Figure 3. 3. Homogeneous translation transformation.

3.4.2. Homogeneous rotation transformation

The simple rotation of the angle β (equation 3.14) around an axis of the reference system is expressed by a matrix with 4 rows and 4 columns (Bajd et al., 2010; Martínez & Campa, 2021). In this matrix, the column expressing the verso around which the rotation occurs remains constant. The other two columns represent the versors rotated by the angle β with respect to the original direction. The fourth column is null because the rotation transformation only changes the directions of the axes (figure 3.4).



$$R(\alpha, x) \cdot G = \begin{bmatrix} 1 & 0 & 0 & 0 \\ 0 & \cos\alpha & \sin\alpha & 0 \\ 0 & -\sin\alpha & \cos\alpha & 0 \\ 0 & 0 & 0 & 1 \end{bmatrix} \cdot \begin{bmatrix} n_x & o_x & a_x & p_x \\ n_y & o_y & a_y & p_y \\ n_z & o_z & a_z & p_z \\ 0 & 0 & 0 & 1 \end{bmatrix}$$

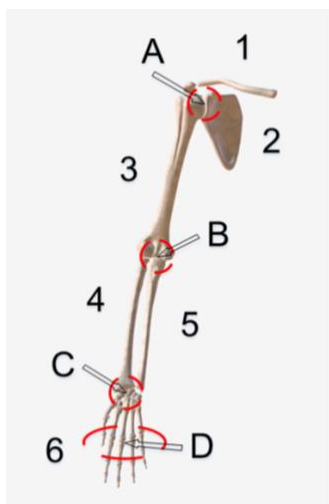
$$= \begin{bmatrix} n_x & o_x & a_x & p_x \\ n_y \cos\alpha - n_z \sin\alpha & o_y \cos\alpha - o_z \sin\alpha & a_y \cos\alpha - a_z \sin\alpha & p_y \cos\alpha - p_z \sin\alpha \\ n_y \sin\alpha + n_z \cos\alpha & o_y \sin\alpha + o_z \cos\alpha & a_y \sin\alpha + a_z \cos\alpha & p_y \sin\alpha + p_z \cos\alpha \\ 0 & 0 & 0 & 1 \end{bmatrix} \quad (3.16)$$

Figure 3. 4. Homogeneous rotational transformation around the Oy axis of the reference system.

3.5. Kinematics of the human upper limb

3.5.1. Anatomical considerations

The kinematic chain of the human upper limb (figure 3.5) consists of the girdle of the upper limb (clavicle and scapula) and the skeleton of the free upper limb (humerus, ulna, radius and carpal bones). In multi-body modeling, the kinematic chain of the human upper limb is structured into rigid assemblies such as the arm, forearm, and hand.



1. clavicle; 2. scapula; 3. the humerus; 4. radius; 5. ulna; 6. the bones of the hand; A. shoulder joint; B. elbow joint; C. hand joint; D. finger joint.

The kinematic elements of the human upper limb are connected by couplings corresponding to anatomical joints. The largest couples in the composition of the human upper limb are (Brahmi et al., 2019; Drăgulescu, 2005; Zhang et al., 2019):

- Shoulder joint: this ball-and-socket joint connects the head of the humerus bone to the glenoid cavity of the scapula. The shoulder joint allows 3 degrees of freedom. The possible moves are:

- flexion-extension
- abduction-adduction
- internal-external rotation.

In a full kinematic model, the shoulder joint is modeled as a superposition of 3 simple rotational couples.

Figure 3. 5. Skeletal and joint structure of the human upper limb

- Elbow joint: from an anatomical point of view, this joint is formed by the overlap of three joints (proximal radioulnar, humeroulnar and humeroradial).

Chapter 3. Kinematic modelling of human upper and lower limbs

From a physiological point of view, the elbow joint behaves as two different couplings that allow the following movements (Dou et al., 2022; Roozbahani et al., 2021):

- flexion-extension;
- pronation-supination.

In kinematic modelling of the human upper limb, the elbow joint is modelled as a superposition of two simple rotational couples. The pronation movement allows an angular variation of 80° , and the supination movement of 85° (Zwerus et al., 2018).

- Hand joint: this joint is perceived as a class III joint that allows the following movements:

- flexion-extension;
- abduction-adduction;
- pronation-supination.

The supination movement accompanies the adduction movement while the pronation movement accompanies the abduction movement.

- Finger joints: compared to the system associated with the lower limbs, they are better structured allowing prehension functions. The finger joints are:

- metacarpophalangeal joints: these are spherical joints that allow 2 degrees of freedom. The movements allowed by these joints are flexion-extension and adduction-abduction (marginal tilt). In kinematic modelling, marginal pitching motion can be neglected due to the small amplitude of the motion. So, we can say that this movement has no significant role in prehension functions.

- proximal and distal interphalangeal joints: they are simple rotational joints that are modelled in kinematics with 1 degree of freedom each. The movements produced in these joints are carried out along transverse axes that pierce the trochlea of the distal extremity of the I and II phalanges. In these joints, flexion-extension movements occur, which involve bringing the fingers closer and closer to the palm.

Complex kinematic models isolate polycell movements from the rest of the anatomical structure. Thus the movement of this segment is considered as a superposition of two rotational movements. The first movement is abduction-adduction, which is performed around the anteroposterior axis that pierces the base of the metacarpal. This movement brings the index finger closer and farther away, respectively. The second movement is the opposition-reposition movement that is performed around the radioulnar axis that passes through the trapezium bone.

3.5.2. Kinematic model of the human upper limb

For the kinematic analysis of the human upper limb, taking into account the anatomical considerations presented previously, we developed a kinematic model characterized by 6 degrees of freedom that can simulate the anatomical behaviour of the human upper limb during biped walking (figure 3.6) (M. Novetschi et al., 2023). Thus, I associated 2 degrees of freedom to the shoulder joint, 1 degree of freedom to the elbow joint, 2 degrees of freedom to the hand joint, and 1 degree of freedom to the finger joint.

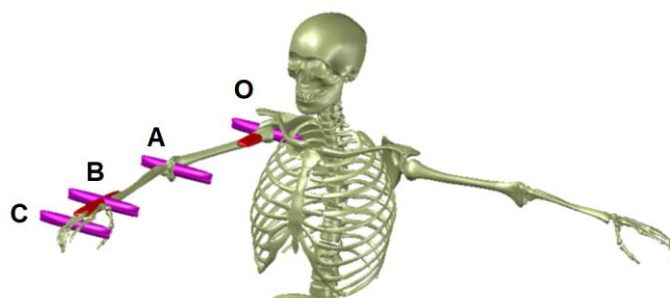


Figure 3. 6. The kinematic model with 6 degrees of freedom of the human upper limb.

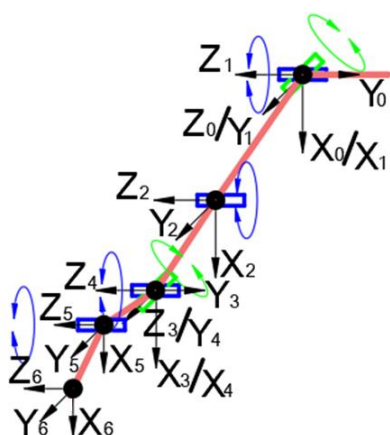


Figure 3. 7. Graphical representation of the coordinate systems associated with the joints of the 6-degree-of-freedom kinematic model of the human upper limb and the effector positioned on the fingertips.

Based on this model, we analyzed the successive positions traversed by an effector positioned on the fingertips. Figure 3.6 shows the kinematic model with 6 degrees of freedom. As can be seen, the shoulder and hand joints are represented as overlays of simple rotational joints. In Figure 3.7, the blue joints allow flexion-extension movements, and the green ones allow abduction-adduction movements. For this study, we considered input data for the simulation, values in correspondence with those from the previously presented norms. According to the specialized literature, the human upper limb is the kinematic chain with the largest active space, a consequence of the kinematic chain configuration (long kinematic element lengths and kinematic torques that allow large rotations).

3.5.3. Mathematical modeling of the human upper limb

Determining the mathematical model for the kinematic analysis of the human upper limb involves following successive stages (M. Novetschi et al., 2023). Thus, in the first stage, we determined the kinematic elements (bones of the upper limb) associated with the studied kinematic chain, as well as the links between them. These links are lower kinematic couples of class V (according to the Denavit-Hartenberg convention). Thus, each joint in the open kinematic chain of the upper limb represents a superposition of simple rotational joints, as follows:

- The shoulder joint is represented as two simple joints of rotation;
- The elbow joint is represented as a simple rotary joint;
- The hand joint is represented as two simple rotary joints;
- The finger joint is represented as a simple rotary joint.

The next stage is determining the coordinate system for the first couple and applying the rules of homogeneous transformations. In this sense, we chose the z_0 axis as the axis of rotation. The other axes were determined using the right-hand rule. Since we chose the z -axis as the axis of rotation, for the calculation of the homogeneous matrix we used the homogeneous rotation transformation ($R(\theta_i, z_{i-1})$) corresponding to the axis in question for all the cups of the system. The next rule applied is that the x -axis must intersect the z -axis of the system in question and that of the previous one. In the case of the base system, the x_0 axis can be chosen arbitrarily. Next, we determined the y_0 axis according to the right-hand rule. Applying these rules we also determined the rest of the systems except for the one associated with the final effector ($O_6x_6y_6z_6$). The axes of this reference system copy the direction and orientation of the axes of the previous system ($O_5x_5y_5z_5$).

The matrices of homogeneous transformations were successively obtained:

$$H_1^0 = \begin{bmatrix} R_1^0 & d_1^0 \\ 0 & 0 & 0 & 1 \end{bmatrix} = \begin{bmatrix} \cos\theta_1 & 0 & \sin\theta_1 & 0 \\ \sin\theta_1 & 0 & -\cos\theta_1 & 0 \\ 0 & 1 & 0 & 0 \\ 0 & 0 & 0 & 1 \end{bmatrix} \quad (3.20)$$

$$H_2^1 = \begin{bmatrix} R_2^1 & d_2^1 \\ 0 & 0 & 0 & 1 \end{bmatrix} = \begin{bmatrix} \cos\theta_2 & 0 & -\sin\theta_2 & l_{\text{humerus}} \cdot \cos\theta_2 \\ \sin\theta_2 & 0 & \cos\theta_2 & l_{\text{humerus}} \cdot \sin\theta_2 \\ 0 & 1 & 0 & 0 \\ 0 & 0 & 0 & 1 \end{bmatrix} \quad (3.24)$$

$$H_3^2 = \begin{bmatrix} R_3^2 & d_3^2 \\ 0 & 0 & 0 & 1 \end{bmatrix} = \begin{bmatrix} \cos\theta_3 & 0 & -\sin\theta_3 & l_{\text{ulna}} \cdot \cos\theta_3 \\ \sin\theta_3 & 0 & \cos\theta_3 & l_{\text{ulna}} \cdot \sin\theta_3 \\ 0 & -1 & 0 & 0 \\ 0 & 0 & 0 & 1 \end{bmatrix} \quad (3.28)$$

$$H_4^3 = \begin{bmatrix} R_4^3 & d_4^3 \\ 0 & 0 & 0 & 1 \end{bmatrix} = \begin{bmatrix} \cos\theta_4 & 0 & \sin\theta_4 & 0 \\ \sin\theta_4 & 0 & -\cos\theta_4 & 0 \\ 0 & 1 & 0 & 0 \\ 0 & 0 & 0 & 1 \end{bmatrix} \quad (3.32)$$

$$H_5^4 = \begin{bmatrix} R_5^4 & d_5^4 \\ 0 & 0 & 0 & 1 \end{bmatrix} = \begin{bmatrix} \cos\theta_5 & -\sin\theta_5 & 0 & l_{\text{degete}}/2 \cdot \cos\theta_5 \\ \sin\theta_5 & \cos\theta_5 & 0 & l_{\text{degete}}/2 \cdot \sin\theta_5 \\ 0 & 0 & 1 & 0 \\ 0 & 0 & 0 & 1 \end{bmatrix} \quad (3.36)$$

$$H_6^5 = \begin{bmatrix} R_6^5 & d_6^5 \\ 0 & 0 & 0 & 1 \end{bmatrix} = \begin{bmatrix} \cos\theta_6 & -\sin\theta_6 & 0 & l_{\text{degete}}/2 \cdot \cos\theta_6 \\ \sin\theta_6 & \cos\theta_6 & 0 & l_{\text{degete}}/2 \cdot \sin\theta_6 \\ 0 & 0 & 1 & 0 \\ 0 & 0 & 0 & 1 \end{bmatrix} \quad (3.40)$$

The matrix H_6^0 is the final homogeneous transformation matrix by which we determined the position of the final effector in a tri-orthogonal system. We have determined this matrix as the matrix product between the homogeneous matrices presented previously (equation 3.41).

$$H_6^0 = \prod_{i=0}^6 H_i^{i-1} \quad (3.41)$$

3.5.4. Pseudocode Algorithm for Positional Analysis of the Human Upper Limb

The basis of the human upper limb positional analysis script is the previously presented mathematical model (equations 3.17 to 3.41), but also algorithm 1 in pseudocode format from table 3.9. As shown in Table 3.9, the algorithm starts by defining the variables x_6^0 , y_6^0 and z_6^0 as null vectors. These vectors contain the successive positions traveled by the effector during the numerical simulation. At the same time, at the beginning of the algorithm, we defined a completion vector necessary for the formation of homogeneous matrices.

The invariable input data (according to the Denavit-Hartenberg convention) for determining the effector positions are the lengths of the kinematic elements such as the

Chapter 3. Kinematic modelling of human upper and lower limbs

humerus, and the ulna, but also the length of the fingers of the hand. In addition to this information, the user must enter from the keyboard the number of analyzed positions, but also the joint parameters ($\theta_1, \theta_2, \theta_3, \theta_4, \theta_5$ and θ_6). The joint parameters are variable and refer to the rotation angles described during the numerical simulation. Based on these data, of the displacement matrices (d_i^{i-1}), of the rotation matrices ($r_i^{i-1} = R(\theta_i, z_{i-1})$), but also of the orientation (I_i^{i-1}) the final homogeneous matrix is determined, as a product between all homogeneous matrices (equation 3.41). The algorithm provides a function (human_upper_limb_6DoF) that contains the previous mathematical model (lines 4 to 33), a function that is executed in a **for** loop that runs according to the number of positions entered by the user from the keyboard (lines 34 and 35).

Tabel 3. 1. Algorithm 1.

Algorithm 1. Positional analysis of the human upper limb characterized by 6 degrees of freedom	
1	$(x_6^0, y_6^0, z_6^0) \leftarrow$ "defining null vectors"
2	$(0, 0, 0, 1) \leftarrow$ "complement vector definition"
3	<i>number of analyzed positions, humerus length, ulna length, finger length</i> \leftarrow <i>user input</i>
4	<i>human_upper_limb_6DoF</i> \leftarrow <i>function definition</i>
5	$(\theta_1, \theta_2, \theta_3, \theta_4, \theta_5, \theta_6) \leftarrow$ <i>user input</i>
6	# defining the 2 degrees of freedom associated with the shoulder joint
7	# define flexion-extension movement
8	$(r_1^0, l_1^0, d_1^0) \leftarrow$ <i>define matrix and vector components</i>
9	$(r_1^0, l_1^0) \leftarrow R_1^0$
10	$(R_1^0, d_1^0) \leftarrow H_1^0$
11	# adduction abduction movement definition
12	$(r_2^1, l_2^1, d_2^1) \leftarrow$ <i>define matrix and vector components</i>
13	$(r_2^1, l_2^1) \leftarrow R_2^1$
14	$(R_2^1, d_2^1) \leftarrow H_2^1$
10	# defining the degree of freedom associated with the elbow joint – flexion-extension movement
16	$(r_3^2, l_3^2, d_3^2) \leftarrow$ <i>define matrix and vector components</i>
17	$(r_3^2, l_3^2) \leftarrow R_3^2$
18	$(R_3^2, d_3^2) \leftarrow H_3^2$
19	# defining the 2 degrees of freedom associated with the hand joint
20	# define flexion-extension movement
21	$(r_4^3, l_4^3, d_4^3) \leftarrow$ <i>define matrix and vector components</i>
22	$(r_4^3, l_4^3) \leftarrow R_4^3$
23	$(R_4^3, d_4^3) \leftarrow H_4^3$
24	# adduction abduction movement definition
20	$(r_5^4, l_5^4, d_5^4) \leftarrow$ <i>define matrix and vector components</i>
26	$(r_5^4, l_5^4) \leftarrow R_5^4$
27	$(R_5^4, d_5^4) \leftarrow H_5^4$
28	# defining the degree of freedom associated with the finger joint – flexion – extension movement
29	$(r_6^5, l_6^5, d_6^5) \leftarrow$ <i>define matrix and vector components</i>
30	$(r_6^5, l_6^5) \leftarrow R_6^5$

31		$(R_6^5, d_6^5) \leftarrow H_6^5$
32		$\prod_{i=0}^6 H_i^{i-1} \leftarrow H_6^0$
33		$(x_6^0, y_6^0, z_6^0) \leftarrow \text{return}$
34	for $i \in [0, \text{număr de poziții}]$ do	
30		membrul_superior_uman_6DoF
36		$(x_6^0, y_6^0, z_6^0) \leftarrow \text{print}$

3.5.5. Results of the human upper limb positional analysis algorithm

The mathematical algorithm presented above was tested under 3 different conditions regarding the number of degrees of freedom associated with the kinematic chain of the human upper limb (2DoF, 4DoF, and 6DoF) (M. Novetschi et al., 2023). Ten successive positions were analyzed for each case. For the created model, the number of degrees of freedom can vary by restricting one or more movements ($\theta_i=0$). The lengths of the kinematic elements are input variables for the mathematical model.

3.5.5.1 The kinematic chain of the human upper limb characterized by 2 degrees of freedom (2DoF)

Figure 3.8 describes the in-plane movement of the effector through a 2D, respectively 3D representation for the first case. The intervals by which the 6 joints vary are presented in table 3.11. According to the resulting data, the trajectory of the effector is generated by the rotational movements of the shoulder and wrist joints along an axis perpendicular to the frontal plane $x_0O_0y_0$. The movement of the effector is relative to the origin of the system $O_0x_0y_0z_0$. The rotational movement around the axis O_0z_0 (figure 3.8 b.) is described in the plane $x_0O_0y_0$ (figure 3.8 a.). All 10 successive positions described by the effector are shown in Figure 3.8. The movement of the effector is described by the increase in the value of the articular parameters, followed by the decrease and implicitly the return to the initial resting position (table 3.11). The final position (table 3.11 - Pos.10) is superimposed with the initial position (table 3.11 - Pos.1) when all parameters of kinematic couples are equal to 00. The motion that the end effector simulates in this case (2 degrees of freedom) is similar to the abduction-adduction motion.

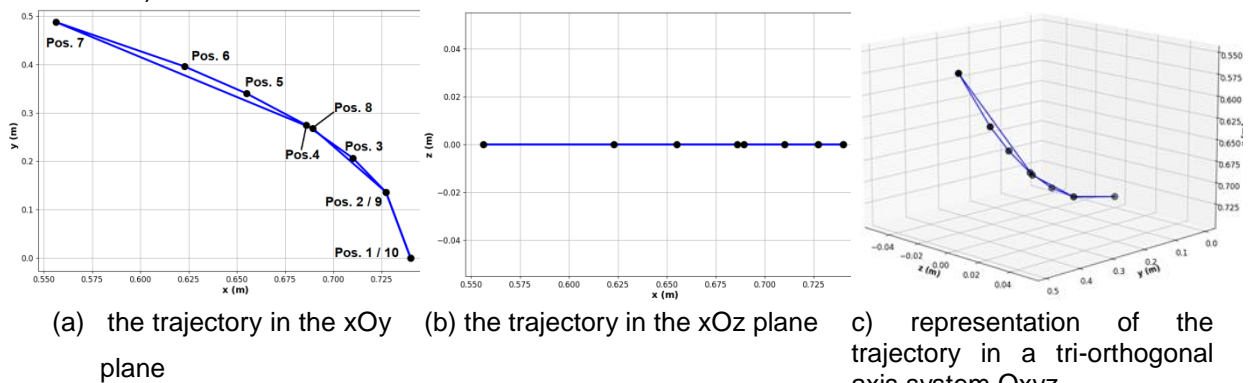


Figure 3. 1. Trajectory of the effector for the case of the kinematic chain with 2 degrees of freedom

3.5.5.2. The kinematic chain of the human upper limb characterized by 4 degrees of freedom (4DoF)

Conform traiectoriei efectorului, deplasarea este proiectată în acest caz în planul sagital (xOz). Acest comportament se datorează faptului că toate elementele cinematice se rotesc în jurul unei axe perpendiculare (Oy) pe planul xOz. Mai exact, este vorba de planul de referință $x_0O_0z_0$ (figura 3.9). În acest caz, membrul superior realizează mișcare de flexie-extensie în toate articulațiile lanțului cinematic (umăr, cot, încheietură și degete). Astfel, membrul superior uman se comportă ca un lanț cinematic cu 4 grade de libertate

Chapter 3. Kinematic modelling of human upper and lower limbs

asociate cu mișcările de flexie-extensie. În acest caz, celelalte mișcări posibile, abducție și adducție sunt blocate.

According to the trajectory of the effector, the displacement is projected in this case in the sagittal plane (xOz). This behavior is due to the fact that all kinematic elements rotate around the axis of an axis perpendicular (Oy) to the xOz plane. More precisely, it is the reference plane $x_0O_0z_0$ (figure 3.9). In this case, the upper limb performs a flexion-extension movement in all joints of the kinematic chain (shoulder, elbow, wrist, and fingers). Thus, the human upper limb behaves as a kinematic chain with 4 degrees of freedom associated with flexion-extension movements. In this case, the other possible movements, abduction and adduction, are blocked.

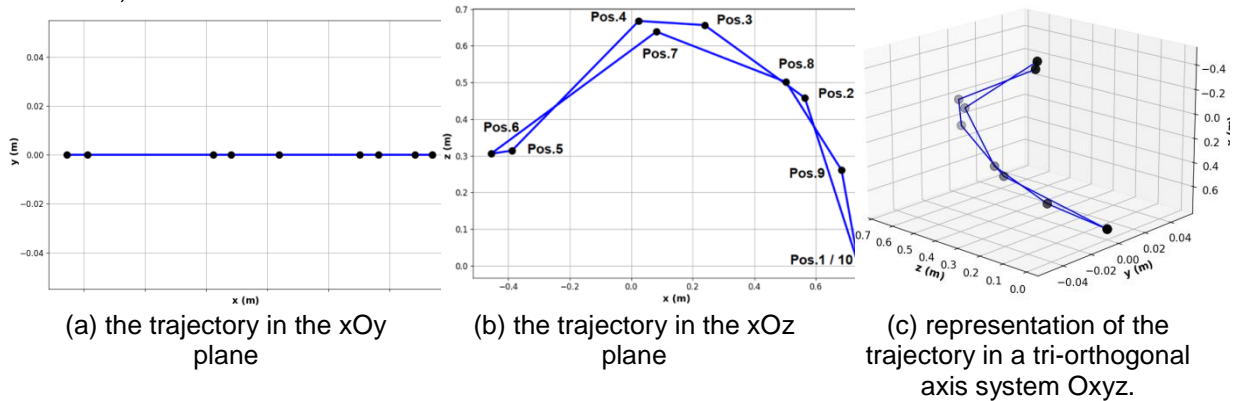


Figure 3. 2. Trajectory of the effector for the case of the kinematic chain with 4 degrees of freedom

3.5.5.3. The kinematic chain of the human upper limb characterized by 6 degrees of freedom (6DoF)

Compared to the two cases presented previously, the upper limb kinematic chain characterized by 6DoF is more complex in terms of effector displacement, since all 6 joints (movements) are active and its trajectory describes projections in all three reference planes (figure 3.10). This kinematic chain is a spatial kinematic chain.

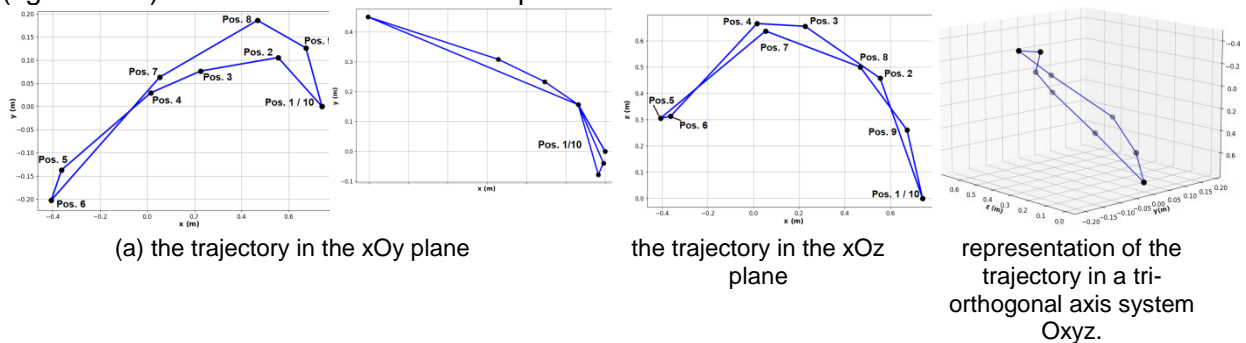


Figure 3. 3. Trajectory of the effector in the case of the kinematic chain with 6 degrees of freedom

3.6. The kinematic model of the human lower limb

3.6.1. Anatomical considerations

At the base of the locomotor system, there are mainly three systems (articular, muscular, and bone). As for the skeletal system, it consists of the pelvic girdle and the bones of the lower limb: femur, patella, tibia, fibula, and finger bones (figure 3.11). Locomotion (the main function of the locomotor apparatus) represents the successive transition from one orthostatic position to another through self-propulsion in the space of kinematic elements

Chapter 3. Kinematic modelling of human upper and lower limbs

(Dragulescu, 2005). The skeleton of the lower limbs is composed of: the bones of the pelvic girdle, the thigh, the calf, and the bones of the foot. The joints between the bones of the pelvic girdle, sacrum, and coccyx, do not allow large relative movements. In dynamic modeling, these displacements are canceled.

The coxal bone is made up of three bones, the ilium, the pubis, and the ischium, which ensure its elasticity. At the level of the thigh, two bones are distinguished. The femur is the longest bone of the human body and the patella (patella) is a short, flattened bone located in the continuation of the femur. The leg is represented by two bones: the tibia and the fibula (fibula). In the composition of the skeleton of the free lower limb, in addition to the femur, patella, tibia, and fibula, the bones of the tarsus, metatarsus, and phalanges are also found.

For the kinematic modeling of the lower limb, all rigid anatomical elements with large displacements (thigh, calf, leg) whose anatomical joints will be associated with kinematic couplings are taken into account.

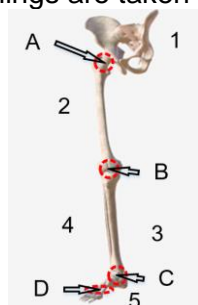


Figure 3. 11. Skeletal and joint structure of the human lower limb

1. the pelvis; 2. the femur; 3. tibia; 4. fibula; 5. bones of the leg; A. coxofemoral joint; B. knee joint; C. ankle joint; D. finger joint.

The joint system of the human lower limb (figure 3.11) consists of:

- The coxofemoral joint. Due to the femoral neck and its inclination at the level of this joint, the following movements can be made:

- flexion – extension;
- abduction - adduction;
- internal – external rotation.

In 2016, Marnee J. McKay and colleagues created a benchmark for isometric strength and joint flexibility. The authors established reference values for the isometric strength of 12 muscle groups and flexibility of 13 common movements in 1,000 subjects. At the same time, they also investigated the influence of demographic and anthropometric factors.

- The knee joint is the largest joint in the structure of the human body. Mechanically, the knee joint plays an important role in both stability and dynamics. This joint is the most stressed joint, both in the orthostatic position and during locomotion, a fact that accentuates the wear of its component elements. The menisci of the knee have a role in the absorption of mechanical shocks and contribute to the lubrication of cartilaginous surfaces. From the point of view of mobility, the knee joint has 3 degrees of freedom. The characteristic movements are:

- flexion – extension;
- internal rotation (amplitude of 5 – 10°) – external (amplitude of 40°);
- lateral–medial inclination.

- The ankle joint is a superposition of three kinematic couples. The first couple is the tibiofibular one where sliding movements are especially produced. From the point of view of kinematic modeling, this joint does not play a special role. The other two joints are the talocrural (cylindrical joint) and talotarsal. The movements allowed by these joints are:

- dorsi flexion - plantar flexion;
- internal rotation (adduction) – external (abduction);
- inversion - eversion; eversion is a combination of abduction, pronation, and flexion, and inversion is a combination of adduction, supination, and extension.

- Joint of the fingers: within this anatomical structure there are the metatarsophalangeal and interphalangeal joints that allow flexion-extension movements of the fingers. In the case of the metatarsophalangeal joints, the flexion-extension movement is accompanied by the abduction-adduction movement. The condition is that the fingers are outstretched. In addition to these movements, there are also internal and external rotations, movements neglected in foot modeling.

3.6.2. The kinematic model of the human lower limb

Thus, we developed an open kinematic chain model with 6 degrees of freedom that can simulate the anatomical behavior of the human lower limb during biped walking (figure 3.12). The proposed model has 4 solid kinematic elements articulated by 6 fifth-class kinematic couples. Thus, I associated 2 degrees of freedom to the hip joint, 1 degree of freedom to the knee joint, 2 degrees of freedom to the ankle joint, and 1 degree of freedom to the finger joint. Based on this model, we analyzed the successive positions traveled by an effector positioned on the tip of the foot. Figure 3.12 shows the kinematic model with 6 degrees of freedom. As can be seen, the coxofemoral joint is considered a superposition of two simple rotational couples, as is the ankle joint.

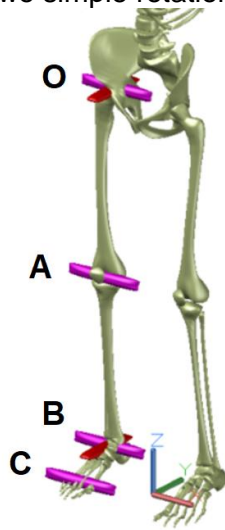


Figura 3. 4. The 6-degree-of-freedom kinematic model of the human lower limb

In figure 3.13 we presented the coordinate systems associated with the 6 studied joints associated with the human lower limb. The origin of the studied anatomical system ($O_0X_0Y_0Z_0$) is located in the coxofemoral (hip) joint. The other systems are positioned in pairs with the origins shifted according to the anatomical dimensions of the kinematic elements (table 3.19). The kinematic elements (bone system) are considered in this case as rigid elements. The $O_6X_6Y_6Z_6$ coordinate system copies the orientation of the $O_5X_5Y_5Z_5$ system and represents the position of the effector positioned on the tip of the foot. As in the case of the model presented previously, the z_i -axes for $i \in [0,5]$ are the axes associated with the rotational movements allowed by the 6 rotational couples.

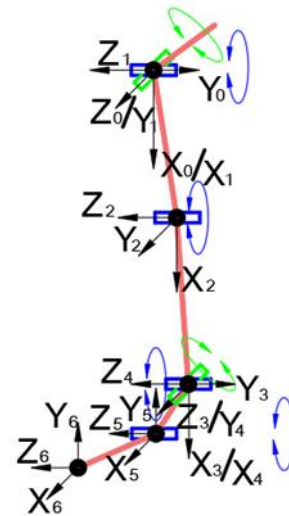


Figura 3. 5. Graphical representation of the coordinate systems associated with the 6-degree-of-freedom kinematic model of the human lower limb and the effector positioned on the tip of the foot.

According to specialized literature, the human lower limb is the kinematic chain (open or closed depending on positioning) with the highest degree of loading.

3.6.3. Mathematical modeling of the human lower limb

For the mathematical modeling of the human lower limb, we defined the kinematic elements of the human lower limb, as well as the kinematic couples. All kinematics are considered rigid and each coupling is described as Class V. The mathematical model has 6 degrees of freedom as follows:

The coxofemoral joint is represented as a superposition of two fifth-class rotation couples;

The knee joint is represented as a fifth-class rotational couple;

The ankle joint is represented as a superposition of two fifth-class rotation couples;

The finger joint is represented as a 5th-class rotational couple.

Next, we determined the coordinate system for the first couple. Thus, the rotation couple in the coxofemoral joint that produces the abduction-adduction movement allows the

Chapter 3. Kinematic modelling of human upper and lower limbs

system to rotate along the z_0 axis. The other axes were determined using the right-hand rule. Since we chose the z -axis as the axis of rotation, for the calculation of the homogeneous matrix we used the homogeneous rotation transformation ($R(\theta_i, z_{i-1})$) corresponding to the axis in question for all the cups of the system (equation 3.15). In equation 3.15, θ_i represents the joint rotation parameter. The next rule applied is that the x -axis must intersect the z -axis of the system in question and that of the previous one. In the case of the base system, the x_0 axis can be chosen arbitrarily. Next, we determined the y_0 axis according to the right-hand rule. Applying these rules we also determined the rest of the systems except for the one associated with the effector positioned on the top of the foot ($O_6x_6y_6z_6$). The axes of this reference system copy the direction and orientation of the axes of the previous system ($O_5x_5y_5z_5$). We successively obtained:

$$H_1^0 = \begin{bmatrix} R_1^0 & d_1^0 \\ 0 & 0 & 0 & 1 \end{bmatrix} = \begin{bmatrix} \cos\theta_1 & 0 & \sin\theta_1 & 0 \\ \sin\theta_1 & 0 & -\cos\theta_1 & 0 \\ 0 & 1 & 0 & 0 \\ 0 & 0 & 0 & 1 \end{bmatrix} \quad (3.45)$$

$$H_2^1 = \begin{bmatrix} R_2^1 & d_2^1 \\ 0 & 0 & 0 & 1 \end{bmatrix} = \begin{bmatrix} \cos\theta_2 & -\sin\theta_2 & 0 & l_{femur} \cdot \cos\theta_2 \\ \sin\theta_2 & \cos\theta_2 & 0 & l_{femur} \cdot \sin\theta_2 \\ 0 & 0 & 1 & 0 \\ 0 & 0 & 0 & 1 \end{bmatrix} \quad (3.49)$$

$$H_3^2 = \begin{bmatrix} R_3^2 & d_3^2 \\ 0 & 0 & 0 & 1 \end{bmatrix} = \begin{bmatrix} \cos\theta_3 & 0 & -\sin\theta_3 & l_{tibia} \cdot \cos\theta_3 \\ \sin\theta_3 & 0 & \cos\theta_3 & l_{tibia} \cdot \sin\theta_3 \\ 0 & -1 & 0 & 0 \\ 0 & 0 & 0 & 1 \end{bmatrix} \quad (3.53)$$

$$H_4^3 = \begin{bmatrix} R_4^3 & d_4^3 \\ 0 & 0 & 0 & 1 \end{bmatrix} = \begin{bmatrix} \cos\theta_4 & 0 & \sin\theta_4 & 0 \\ \sin\theta_4 & 0 & -\cos\theta_4 & 0 \\ 0 & 1 & 0 & 0 \\ 0 & 0 & 0 & 1 \end{bmatrix} \quad (3.57)$$

$$H_5^4 = \begin{bmatrix} R_5^4 & d_5^4 \\ 0 & 0 & 0 & 1 \end{bmatrix} = \begin{bmatrix} \cos\theta_5 & -\sin\theta_5 & 0 & (l_{degete}/2) \cdot \sin\theta_5 \\ \sin\theta_5 & \cos\theta_5 & 0 & (l_{degete}/2) \cdot \cos\theta_5 \\ 0 & 0 & 1 & 0 \\ 0 & 0 & 0 & 1 \end{bmatrix} \quad (3.61)$$

$$H_6^5 = \begin{bmatrix} R_6^5 & d_6^5 \\ 0 & 0 & 0 & 1 \end{bmatrix} = \begin{bmatrix} \cos\theta_6 & -\sin\theta_6 & 0 & (l_{degete}/2) \cdot \sin\theta_6 \\ \sin\theta_6 & \cos\theta_6 & 0 & (l_{degete}/2) \cdot \cos\theta_6 \\ 0 & 0 & 1 & 0 \\ 0 & 0 & 0 & 1 \end{bmatrix} \quad (3.65)$$

The position in a tri-orthogonal system of the effector positioned on the tip of the foot is given by the homogeneous transformation matrix (H_6^0).

$$H_6^0 = \prod_{i=0}^6 H_i^{i-1} = H_1^0 \cdot H_2^1 \cdot H_3^2 \cdot H_4^3 \cdot H_5^4 \cdot H_6^5 \quad (3.66)$$

3.6.4. Pseudocode Algorithm for Positional Analysis of the Human Lower Limb

To solve the described model, I created a script in the Python programming language, the script is presented as a pseudocode algorithm in table 3.20. In principle, Algorithm 2 follows the logic presented for the previous algorithm. As shown in Table 3.20, the algorithm starts by defining the variables x_6^0 , and z_6^0 as null vectors. These vectors contain the successive positions traveled by the effector positioned in this case on the tip of the foot. Since homogeneous matrices contain 4 rows and 4 columns, we defined a complement vector for this. According to the Denavit-Hartenberg convention, the invariant input data for calculating the effector positions are the lengths of the rigid kinematic elements (femur, tibia, and leg bones). The joint parameters referring to the rotation angles along the considered axes ($\theta_1, \theta_2, \theta_3, \theta_4, \theta_5$, and θ_6) are also input data to be entered by the user from the keyboard. Based on these data, a matrix pre-calculation is performed to determine the rotation matrices ($r_i^{i-1} = R(\theta_i, z_{i-1})$). The determination of the homogeneous matrices responsible for each rotation presupposes the first phase definition of the orientation matrices (I_i^{i-1}) and the displacement vectors (d_i^{i-1}).

We determined the final homogeneous matrix as the product between all homogeneous matrices ($H_6^0 = \prod_{i=0}^6 H_i^{i-1}$). The algorithm provides a function (human_lower_limb_6DoF) that contains the previous mathematical model (lines 4 to 33), a function that is executed in a for loop that runs according to the number of positions entered by the user from the keyboard (lines 34 and 35).

Pentru rezolvarea modelului descris, am realizat un script în limbajul de programare Python, script prezentat sub formă de algoritm pseudocod în tabelul 3.20. În principiu, algoritmul 2 urmărește logica prezentată pentru algoritmul precedent. Așa cum este prezentat în tabelul 3.20, algoritmul începe cu definirea variabilelor x_6^0 , y_6^0 și z_6^0 ca vectori nuli. Acești vectori conțin pozițiile succesive parcurse de efectorul poziționat în acest caz pe vârful piciorului. Deoarece matricele omogene conțin 4 rânduri și 4 coloane, am definit în acest sens un vector de completare. Conform convenției Denavit-Hartenberg, datele de intrare invariabile pentru calculul pozițiilor efectorului sunt lungimile elementelor cinematice rigide (femur, tibia și oasele piciorului). Parametrii articulari ce fac referire la unghiurile de rotație după axele considerate ($\theta_1, \theta_2, \theta_3, \theta_4, \theta_5$ și θ_6) sunt, de asemenea, date de intrare ce trebuie introduse de către utilizator de la tastatură. Pe baza acestor date se realizează un pre-calcul matriceal pentru determinarea matricelor de rotație ($r_i^{i-1} = R(\theta_i, z_{i-1})$). Determinarea matricelor omogene responsabile pentru fiecare rotație presupune definirea în primă fază a matricelor de orientare (I_i^{i-1}) și a vectorilor de deplasare (d_i^{i-1}).

Matricea omogenă finală am determinat-o ca produs între toate matricele omogene ($H_6^0 = \prod_{i=0}^6 H_i^{i-1}$). Algoritmul prevede o funcție (membrul_inferior_uman_6DoF) ce conține modelul matematic anterior (liniile de la 4 la 33), funcție ce este executată într-o buclă de tip **for** ce rulează în funcție de numărul de poziții introduse de utilizator de la tastatură (liniile 34 și 35).

Tabel 3. 2. Algorithm 2.

Algorithm 2. Positional analysis of the human lower limb characterized by 6 degrees of freedom	
1	$(x_6^0, y_6^0, z_6^0) \leftarrow$ defining null vectors
2	$(0, 0, 0, 1) \leftarrow$ define complement vector "
3	number of analyzed positions, femur length, tibia length, finger length \leftarrow user input
4	human_lower_limb_6DoF \leftarrow function definition
5	$(\theta_1, \theta_2, \theta_3, \theta_4, \theta_5, \theta_6) \leftarrow$ user input
6	# defining the 2 degrees of freedom associated with the hip joint
7	# define flexion-extension movement
8	$(r_1^0, l_1^0, d_1^0) \leftarrow$ define matrix and vector components

9		$(r_1^0, l_1^0) \leftarrow R_1^0$
10		$(R_1^0, d_1^0) \leftarrow H_1^0$
11		# definire mișcare de adducție-abducție
12		$(r_2^1, l_2^1, d_2^1) \leftarrow$ define matrix and vector components
13		$(r_2^1, l_2^1) \leftarrow R_2^1$
14		$(R_2^1, d_2^1) \leftarrow H_2^1$
15		# defining the degree of freedom associated with the knee joint – flexion – extension movement
16		$(r_3^2, l_3^2, d_3^2) \leftarrow$ define matrix and vector components
17		$(r_3^2, l_3^2) \leftarrow R_3^2$
18		$(R_3^2, d_3^2) \leftarrow H_3^2$
19		# defining the 2 degrees of freedom associated with the ankle joint
20		# define flexion-extension movement
21		$(r_4^3, l_4^3, d_4^3) \leftarrow$ define matrix and vector components
22		$(r_4^3, l_4^3) \leftarrow R_4^3$
23		$(R_4^3, d_4^3) \leftarrow H_4^3$
24		# adduction abduction movement definition
25		$(r_5^4, l_5^4, d_5^4) \leftarrow$ define matrix and vector components
26		$(r_5^4, l_5^4) \leftarrow R_5^4$
27		$(R_5^4, d_5^4) \leftarrow H_5^4$
28		# defining the degree of freedom associated with the finger joint – flexion – extension movement
29		$(r_6^5, l_6^5, d_6^5) \leftarrow$ define matrix and vector components
30		$(r_6^5, l_6^5) \leftarrow R_6^5$
31		$(R_6^5, d_6^5) \leftarrow H_6^5$
32		$\prod_{i=0}^6 H_i^{-1} \leftarrow H_6^0$
33		$(x_6^0, y_6^0, z_6^0) \leftarrow$ return
34		for $i \in [0, \text{număr de poziții}]$ do
35		membrul_inferior_uman_6DoF
36		$(x_6^0, y_6^0, z_6^0) \leftarrow$ print

3.6.5. Results of the human lower limb positional analysis algorithm

The mathematical algorithm for analyzing the kinematics of the human lower limb, presented above, was compiled in 3 different cases. The cases differ according to the number of degrees of freedom associated with the kinematic chain of the human lower limb (2DoF, 4DoF, and 6DoF). For each case we analyzed ten successive positions. For the created model, the number of degrees of freedom can vary by blocking a movement, respectively a joint ($\theta_i=0$). The lengths of the kinematic elements of the human lower limb are measured on a random subject and are input variables for the mathematical model.

3.6.5.1. Kinematic chain of the human lower limb characterized by 2 degrees of freedom (2DoF)

Figure 3.14 describes the movement in the frontal plane of the effector through a 2D and 3D representation respectively for the first case. The resulting data show that the

Chapter 3. Kinematic modelling of human upper and lower limbs

effector trajectory is generated by the rotational movements of the hip and ankle joints along an axis perpendicular to the frontal plane $x_0O_0y_0$. The 10 successive positions described by the effector in this case are shown in figure 3.14. The movement of the effector in the top of the foot is described by the increase in the value of the joint parameters, followed by the decrease and implicitly the return to the initial state of rest. The motion that the end effector simulates in this case (2 degrees of freedom) is similar to the abduction-adduction motion in the hip and ankle joints.

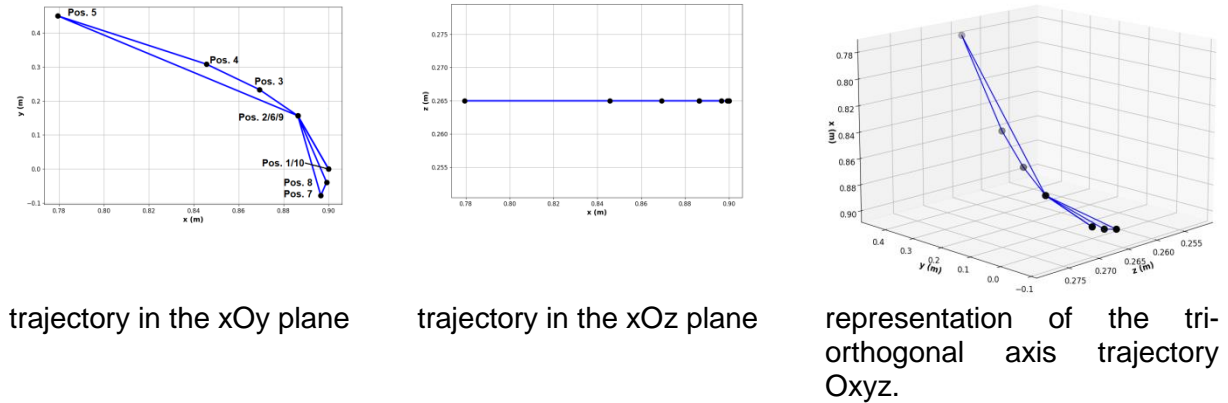


Figure 3. 14. Trajectory of the effector for the case of the kinematic chain with 2 degrees of freedom

3.6.5.2. The kinematic chain of the human lower limb characterized by 4 degrees of freedom (4DoF)

Conform traiectoriei efectorului, deplasarea membrul inferior este proiectată în acest caz în planul sagital (xOz), figura 3.15 b. Acest comportament se datorează faptului că toate elementele cinematice se rotesc în jurul unei axe perpendiculare (Oy) pe planul xOz . Mai exact, este vorba de planul de referință $x_0O_0z_0$ (figura 3.15). În acest caz, membrul inferior realizează mișcare de flexie-extensie în toate articulațiile lanțului cinematic (șold, genunchi, gleznă și degete). În acest caz, membrul inferior uman se comporta ca un lanț cinematic cu 4 grade de libertate asociate cu mișcările de flexie-extensie. Celelalte mișcări posibile, abducție și adducție, sunt blocate (figura 3.15 a).

According to the trajectory of the effector, the displacement of the lower limb is projected in this case in the sagittal plane (xOz), figure 3.15 b. This behavior is because all kinematic elements rotate around a perpendicular axis (Oy) on the xOz plane. More precisely, it is the reference plane $x_0O_0z_0$ (figure 3.15). In this case, the lower limb performs a flexion-extension movement in all joints of the kinematic chain (hip, knee, ankle and fingers). In this case, the human lower limb behaves as a kinematic chain with 4 degrees of freedom associated with flexion-extension movements. The other possible movements, abduction and adduction, are blocked (figure 3.15 a).

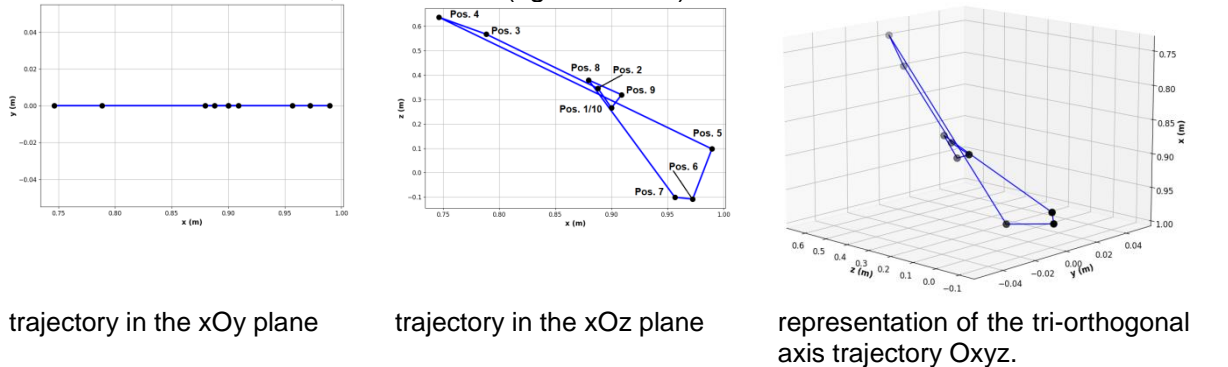
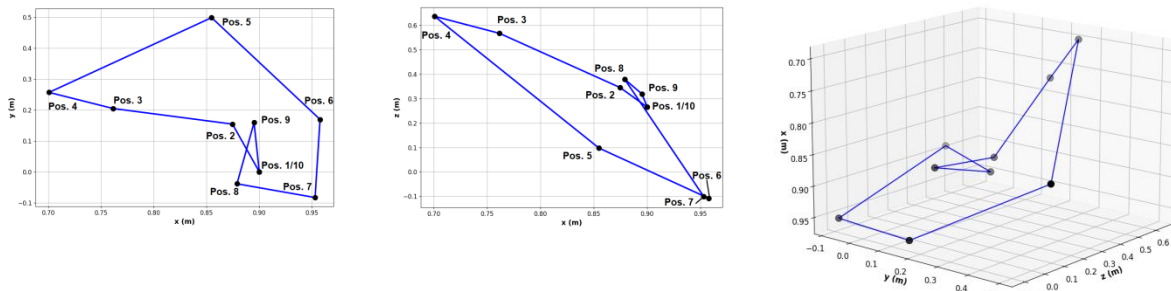


Figure 3. 6. Trajectory of the effector for the case of the kinematic chain with 4 degrees of freedom

3.6.5.3. The human lower limb kinematic chain characterized by 6 degrees of freedom (6DoF)

This case is characterized by a higher degree of complexity compared to those previously presented. More precisely, the kinematic chain of the lower limb has 6 degrees of freedom and simulates the movement of a space mechanism (figure 3.16 c). The movement of the effector positioned at the end of the lower limb is described in two anatomical planes (figure 3.16). The flexion-extension movement is performed in the sagittal plane (figure 3.16 a), and the abduction-adduction movement in the frontal plane (figure 3.16 b).



trajectory in the xOy plane

trajectory in the xOz plane

representation of the tri-orthogonal axis trajectory Oxyz.

Figure 3. 7. Trajectory of the effector for the case of the kinematic chain with 6 degrees of freedom

3.7. Partial conclusions

In this PhD thesis, I used a new approach in the field of biomechanics to quantify the displacement vector $\vec{r} = r_x\vec{i} + r_y\vec{j} + r_z\vec{k}$ for 3D motion and default = $\vec{r} = r_x\vec{i} + r_y\vec{j}$ and $\vec{r} = r_x\vec{i} + r_z\vec{k}$ for planar motion) resulting from a positional analysis of human kinematic chains. The method addressed is that of homogeneous rotation transformations, a method mainly used in the study of manipulators and robots. This method involves determining the rotation matrix and displacement vector for each studied joint (movement) relative to the reference joint (global reference system $O_0x_0y_0z_0$). The direct result is represented by the scalar components of the displacement vector described by the end effector. The end effector is the theoretical point located at the tip of the toes or fingers.

The movement of the segments of the human body, regardless of the analyzed kinematic chain, is a complex one. Human kinematic chains (lower limbs, upper limbs, trunk, or whole body) can perform planar or spatial movements. However, rarely are the movements produced by kinematic chains exclusively planar. In this case, they can only be considered planar movements if the goal is to simulate certain movements, such as flexion and extension or abduction and adduction. To be able to analyze the movement of the human body as a whole or a part, mathematical models or multi-body models can be used. Mathematical models in this PhD thesis can be adapted so that the degree of complexity increases or decreases.

Thus, planar or spatial movements can be simulated. By blocking the described motions of the kinematic chains, motions of the kinematic chains with one degree of freedom or up to 6 degrees of freedom can be simulated. To increase the complexity of the models (over 6 degrees of freedom) they can be easily adjusted by adding the homogeneous matrices associated with the desired movements to be analyzed. The maximum complexity to which these models can be adjusted without considering phalanx joints is 10 DoF. The 10 degrees of freedom involves the analysis of the main movements performed by the upper or lower kinematic chains.

The mathematical models were developed using the Python programming language, a fast and efficient programming language used by researchers around the world to develop cutting-edge solutions.

CHAPTER 4.

DYNAMIC MODELLING OF THE HUMAN UPPER LIMB

4.1. Introduction

In figure 4.1 we presented the conceptual diagram of the neuro-musculoskeletal system responsible for movement control. The system contains kinematic elements (anatomical segments of the body), actuators (skeletal muscles), sensors (proprioceptive, tactile, visual, auditory, and other sensors), and the controller component (central nervous system). In figure 4.1, the variable τ represents the delays caused by the transport and processing of information in and through the central nervous system.

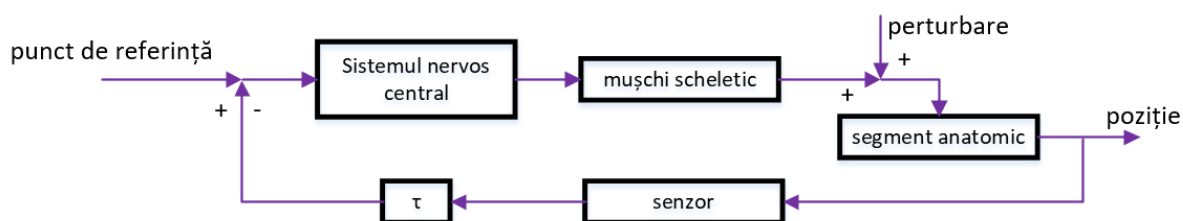


Figure 4. 1. The neuro-musculoskeletal system characteristic of the human body

Next, I will analyze in detail the dynamics of the muscular system. The muscular system is a vital component in the architecture of the human body. Its importance results from the fact that it generates movement, but also protects and supports the vital organs.

The muscular system is the actuator of the body. To study this system, models are needed to identify how a neurological impulse to the muscle results in mechanical energy, that is, a contraction force possibly combined with a displacement of the anatomical segments.

The complex structure of a muscle is not easily characterized by a model. In this sense, assumptions and simplifications are necessary. In this chapter, I analyze how the structure of a muscle is related to its functional properties.

The skeletal muscle system is defined by two types of contractions. Isometric muscle contractions are contractions in which the muscle structure does not change in size. The only variable in this regard is the state of tension. By isometric contraction skeletal muscle does not generate mechanical work. In this case, the potential difference acting on the muscle is finally transformed into heat. The second type of contraction is isotonic. During this contraction, the skeletal muscle changes its geometry (shortens or lengthens). The end product of this contraction is mechanical work and therefore locomotion or various other activities. The forces developed during isotonic or isometric contractions vary from muscle to muscle.

4.2. Skeletal muscular system

4.2.1. The structure of skeletal muscle

Skeletal muscles are also called striated muscles because, at the microscopic level, they have a striated appearance. The skeletal muscle system represents on average 40% of the mass of the human body. The following components are identified in the structure of skeletal muscles (figure 4.2):

- the central area or body of the muscle consists of muscle fibers that can reach lengths between 100 and 150 mm;
- two endings (extremities) called tendons: on the fixed bone it is called origin, and on the mobile one it is called insertion.

4.2.2. Types of contractions specific to skeletal muscle

Voluntary muscle contractility occurs in the form of active force and is often represented schematically by the model of an actuator. Skeletal muscle contraction can be:

- **isometric contraction**: occurs as the muscle develops tension without changing the angle of the joint in question. During isometric contractions, there is a shortening of the sarcomere followed by an increase in muscle force, but not the displacement of the load, because in this case, the force produced cannot overcome the load.

- **concentric isotonic contraction** involves decreasing the length of the muscle fiber to move a load. An example of this is the contraction developed by the biceps brachii muscle when the hand is raised. With the execution of this movement, there is an increase in muscle tension. As the biceps brachii contracts, the angle of the elbow joint decreases as the forearm is brought toward the body. In this case, the biceps brachii contracts and the sarcomeres in its muscle fibers shorten and cross-bridges are formed (myosin ends pull actin) (figure 4.4);

- **eccentric isotonic contraction** occurs as muscle tension decreases and the muscle lengthens. In this case, the hand is lowered in a slow and controlled manner as the number of cross-bridges activated by the nervous system stimulation decreases. When tension is released from the biceps brachii, the angle of the elbow joint increases. Eccentric contractions are used not only for movement but also for body balance (figure 4.5).

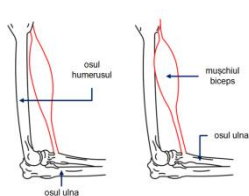


Figure 4. 3. Isometric muscle contraction.

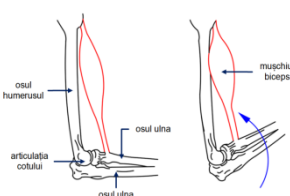


Figure 4. 4. Concentric isotonic muscle contraction

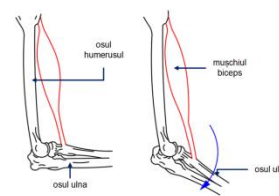


Figure 4. 5. Eccentric isotonic muscle contraction.

4.3. Finite element modeling of skeletal muscle

4.3.1. Parametric considerations of finite element simulation

For the study of the statics and dynamics of biomechanical kinematic chains, determinations of the forces generated by the skeletal muscles are necessary, either

Chapter 4. Dynamic modelling of the human upper limb

experimentally or based on numerical modeling using the finite element method (FEM), a method that can retrieve the mechanical properties of structural elements from experiments.

To determine muscle forces, biomechanics simulations are used in OpenSim Stanford (C. Nguyen & Leonessa, 2014) Matlab programs, but also finite element modeling with dedicated programs created by the authors (Lechosa Urquijo et al., 2022) (analysis linear). At the same time, simulations using programs such as COMSOL or Ansys Workbench can also be used. Simulation modules like Rigid Dynamics and Transient Structural are implemented in Ansys.

The Rigid Dynamics module provides explicit solutions for rigid body dynamics problems, but also for the efficient and robust evaluation of mechanical systems containing complex assemblies of rigid parts interconnected by couplings, subject to a law of motion.

Transient Structural is another module in Ansys Workbench that should not be confused with the Static Structural module. A static structural analysis determines the displacements, stresses, and forces (stresses) in kinematic elements or kinematic chains, stresses caused by loads that do not induce significant inertia and damping effects. On the other hand, a transient structural analysis (also called time history analysis) is used to determine the dynamic response of a structure under time-dependent loads. It can be used to determine the time-varying displacements, strains, stresses, and forces in a structure as it responds to varying loads.

The proposed finite element model for the numerical determination of muscle force was made in the Ansys Workbench program in the Static Structural module.

The modeling of the kinematic elements was done with bar-type elements (BEAM 188) with two nodes and six degrees of freedom per node (three translations and three rotations), while TRUSS-type elements were used for the muscles (figure 4.6).

We studied, using finite element analysis, the mechanical behavior of the biceps brachii muscle for a concentric isotonic contraction. The biceps brachii muscle, formed by the long head and the short head, is a strong flexor of the forearm on the arm, a movement that occurs after an axis of rotation that passes through the elbow joint.

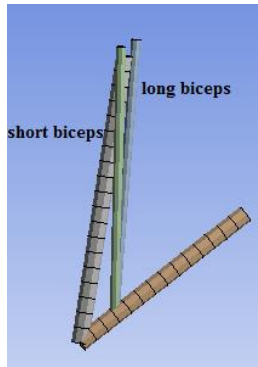


Figure 4. 6.
Discretization with
finite elements

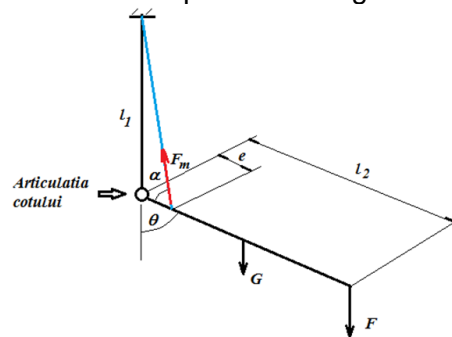


Figure 4. 7. Working diagram.

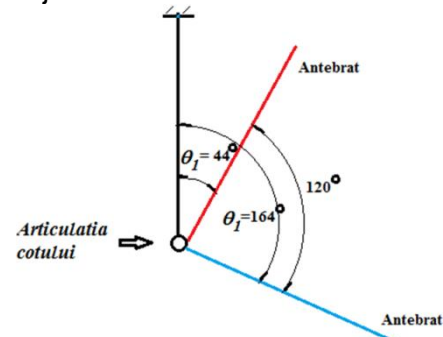


Figure 4. 8. Extreme positions of
the forearm described by the
angle θ .

The mechanical properties taken into consideration in the modeling process of the two bars (forearm and arm bones) that converge in the elbow joint characterized by a degree of freedom are: density (1640 kg/m^3); longitudinal modulus of elasticity ($E=16700\text{MPa}$); Poisson's constant (value of 0.3). The model has implemented the following connection conditions: embedded in the shoulder (fixed support) and in the insertion points on the scapula of the tendons of the two muscles (figure 4.9, element A); simple rotation coupling (connections: Joint Body-body-Revolute) in the elbow joint. For the two biceps muscles considered as a spring and damping model, the numerical values considered from the references (Dereshgi, 2023; GHERASIM & ARGHIR, 2021), are: the elastic constant ($K=3535 \text{ N/m}$); damping coefficient ($c=6916 \text{ Ns/m}$). For the considered movement, the biceps longus and biceps brevis are the largest contributors. A model proposed and used in reference (Lechosa Urquijo et al., 2022) for the two muscles in a linear finite element

Chapter 4. Dynamic modelling of the human upper limb

modeling considers the whole muscle, with tendons, as a bar articulated at the insertion points and stressed only axially (stretch and compression). The material of this articulated bar (in Ansys Link/Truss) that models the two muscles has the following mechanical properties: longitudinal modulus of elasticity ($E=2000\text{MPa}$); Poisson's constant (value of 0.43); cross-sectional area (value of 100 mm^2).

Figure 4.9 shows the boundary conditions (B - forearm weight force of 25 N; C - lifting weight force of 150 N), and figure 4.10 shows the details of the analysis.

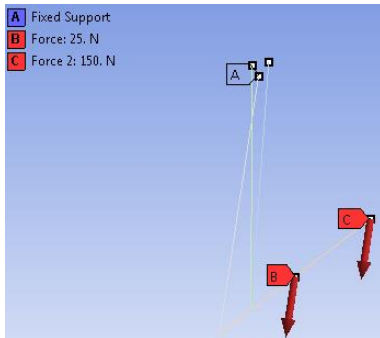


Figure 4. 9. Boundary conditions

Details of "Analysis Settings"	
[-] Step Controls	
Number Of Steps	1.
Current Step Number	1.
Step End Time	1. s
Auto Time Stepping	Program Controlled
[-] Solver Controls	
Solver Type	Program Controlled
Weak Springs	Off
Solver Pivot Checking	Program Controlled
Large Deflection	Off
Inertia Relief	Off
[+] Rotordynamics Controls	
[+] Restart Controls	
[+] Nonlinear Controls	

Figure 4. 10. Details of Static Structural analysis.

4.3.2. Results obtained from finite element analysis

In subchapter 4.3 we analyzed the muscle activity generated by the biceps muscle (short end and long end) during the variation of the articular parameter of the rotation torque in the elbow, as well as their implications on the mechanical system.

Figures 4.11 – 4.23 reflect the total deformations for the modeled mechanical system when the forearm positioning angle varies between 136° - 16° in 10° increments. This variation is done in the simple elbow joint. The simulated motion is similar to that constrained by a hinge.

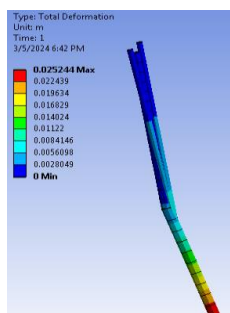


Figure 4. 1. Total deformation for $\theta=16^\circ$.

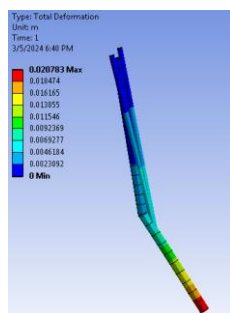


Figure 4. 2. Total deformation for $\theta=26^\circ$.

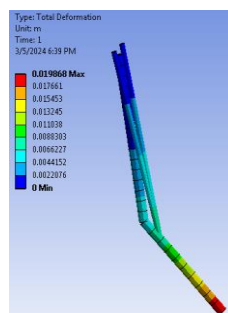


Figure 4. 3. Total deformation for $\theta=36^\circ$.

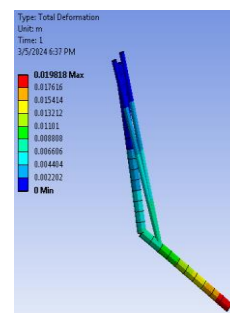


Figure 4. 4. Total deformation for $\theta=46^\circ$.

Chapter 4. Dynamic modelling of the human upper limb

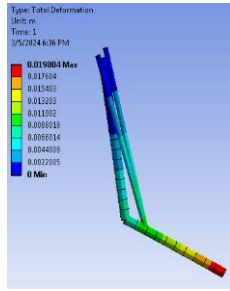


Figure 4. 5. Total deformation for $\theta=56^\circ$.

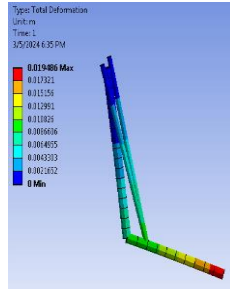


Figure 4. 6. Total deformation for $\theta=66^\circ$.

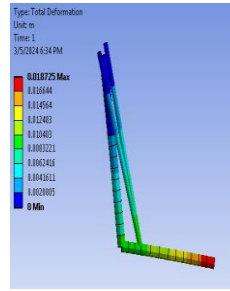


Figure 4. 7. Total deformation for $\theta=76^\circ$.

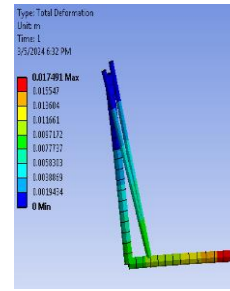


Figure 4. 8. Total deformation for $\theta=86^\circ$.

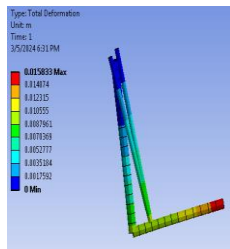


Figure 2 4. 9. Total deformation for $\theta=96^\circ$.

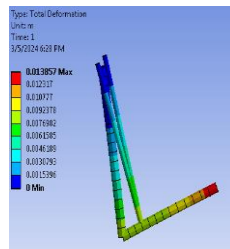


Figure 4. 10. Total deformation for $\theta=106^\circ$.

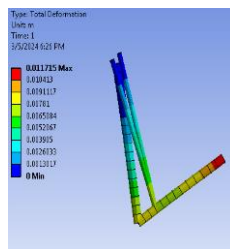


Figure 4. 11. Total deformation for $\theta=116^\circ$.

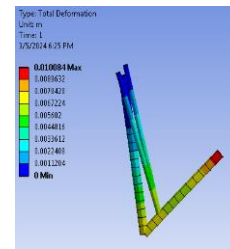


Figure 4. 12. Total deformation for $\theta=126^\circ$.

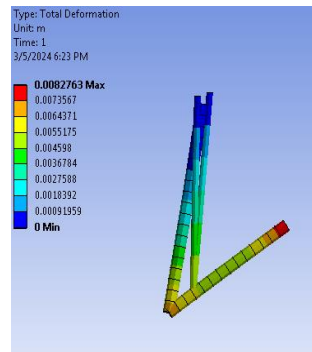


Figure 4. 13. Total deformation for $\theta = 136^\circ$.

4.3.3. The conclusions of the finite element simulation

Figure 4.24 shows the nonlinear variations of the muscle forces developed by the two muscles (biceps long end and biceps short end) about the variation of the angle θ . Applying the polynomial regression method of the 10th degree (equation 4.1) and the specific statistical indicators, ($R^2 = 1$ and $RMSE = 1.126$) it can be seen that there is an increased dependence between the dependent variable (muscle strength) and the independent variable (angle of variation θ). R^2 is the statistical measure that indicates the degree of fit between the independent and the dependent variable.

Figures 4.25 and 4.26 show the variations of the muscle forces described by both ends of the biceps muscle, respectively the long end and the short end. The variation of muscle forces is described as a function of the variation of the flexion-extension angle of the elbow joint. The elbow joint is a simple rotational kinematic coupling. As can be seen in the two figures there is a variation in the opposition in terms of the muscular forces developed. At the same time, it can be observed that mathematical models of polynomial regression of the 10th degree (equation 4.2 for the muscle force described by the biceps long-end muscle and equation 4.3 for the muscle force described by the biceps short-end muscle) reflect

Chapter 4. Dynamic modelling of the human upper limb

increased precision the dependence between muscle activity and the variation of the angle of flexion-extension of the rotation couple in the elbow. In the case of the biceps longus (BCL) the statistical coefficients are $R^2 = 1$ and $RMSE = 0.364$, and for the biceps brevis (BCS) they are $R^2 = 1$ and $RMSE=0.1676$.

Making a comparison with the statistical indicators presented previously, it is observed that the residual values are lower for the 10th-degree polynomials that reflect the variation of the BCL and BCS muscles compared to the resultant force.

The greatest muscle forces for the long-end biceps muscle are for the angle $\theta \in (90^\circ; 110^\circ)$, while for the short biceps muscle, the maximum forces are obtained for the angle $\theta \in (120^\circ; 160^\circ)$. The variation and values of the muscle forces described by the two muscles depend on the considered insertion positions of the tendons. The values of the muscle forces resulting from the finite element analysis are close to those of the model presented in the article (Lechosa Urquijo et al., 2022).

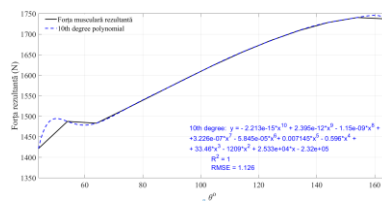


Figure 4. 24. Resultant muscle force.

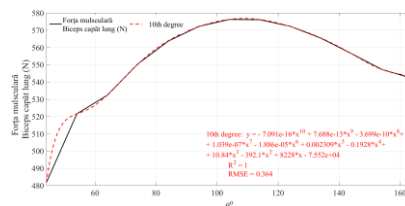


Figure 4. 25. Muscle strength developed by biceps long end.

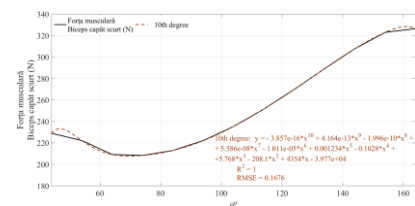


Figure 4. 26. Muscle strength developed by the biceps short end.

The dynamic analysis of forearm movement is based on D'Alembert's principle. According to this principle statically acting forces and inertial forces are in dynamic equilibrium

Figure 4.28 shows the variations of the moments in the elbow joint generated by the action of muscle forces. During the flexion movement of the forearm, the muscles responsible for the variation of the joint parameter θ , are the biceps longus and biceps brevis. The static and dynamic moments show approximately similar variations (figure 2.28). To compare the two moments generated by the muscle forces statically and dynamically, making a representation about the angle θ will obtain curves with the same shape and very close values.

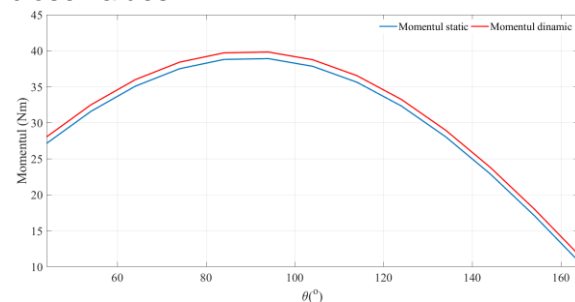


Figure 4. 28. The variation of the static and dynamic moment in relation to the created elbow joint as a function of θ .

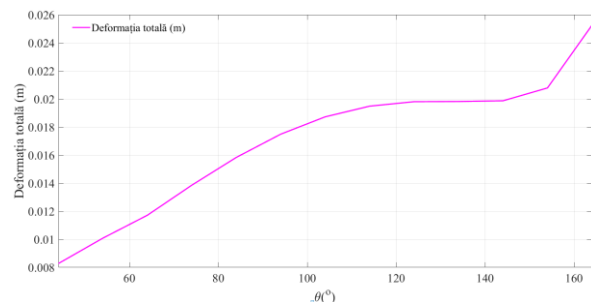


Figure 4. 29. Variation of the total strain as a function of the variation of the angle θ .

A static analysis of the ensemble of forces acting on the bone segments including the forces in the muscles and tendons with their insertion points for different positions is sufficient to establish the magnitude of the muscle forces. Inertia forces in biomechanical systems have a less relevant effect compared to inertia forces in mechanical systems where velocities and accelerations have high values.

Figure 4.29 shows the deformation resulting from the finite element analysis. This deformation is the consequence of the system of forces acting on the considered kinematic elements (arm = humerus length and forearm = ulna length). As can be seen, the resulting

Chapter 4. Dynamic modelling of the human upper limb

moment has a maximum deformation effect of about 26 mm. It should be noted that both the composition and the internal structure of elements in finite element modelling are approximations of reality. The maximum deformation occurs when the flexion angle in the elbow has a maximum value.

4.4. Mathematical model for skeletal muscle analysis

The mathematical model we developed is based on the skeletal muscle analysis model developed by Archibald Vivian Hill. Skeletal muscle is the actuator of the biological body. Skeletal muscle modelling can be structural or phenomenological. In structural modelling, the mechanical and chemical phenomena occurring in the sarcomere are taken into account (Huxley, 1957a). The ability of these models to simulate muscle force is conditioned by the number of cross-bridges between actin myofilaments and myosin and titin. Thus, due to the complexity, structural models are far from being used in the study of human body movements (Arslan et al., 2019).

Phenomenological-type models (Table 4.1), such as Hill's model, are widely used to mimic the mechanical behaviour of motor transfer units (Huxley, 1957b; Zajac, 1989). These models are based on spring and/or damper rheological elements and an element that characterizes the contractile potential of the muscle. The last element refers to the interaction between the proteins underlying the generation of muscle force (Arslan et al., 2019).

The model we used in this chapter consists of four general components (equation 4.8): the contractile element (EC), the series elastic element (EES), the parallel elastic element (EEP), and the tendon (T). EC represents the active, i.e., contractile, properties of the muscle, while EES, EEP, and tendon represent the nonlinear passive stiffness. EES represents the elasticity of actin-myosin cross-bridges, EEP represents the passive elastic properties of muscle fibres and tendons. EES is frequently neglected in inverse dynamics models and can be achieved with little loss of accuracy if the model does not include short-tendon actuators.

In this chapter, we analyzed the force developed by the biceps brachii contractile element. The determination sequence as well as the algorithm are presented in the following. The phenomenological model used to determine muscle activity is presented in figure 4.30. As can be seen, the contractile element is connected in parallel with the EEP element which simulates the visco-elastic behaviour determined by the connective tissues parallel to the muscle fibre. Within the connective tissues, loose, adipose, blood, and cartilaginous ones are identified; bones.

Within the studied model (figure 4.30), the EES element simulates the effect of the tendon on muscle activity.

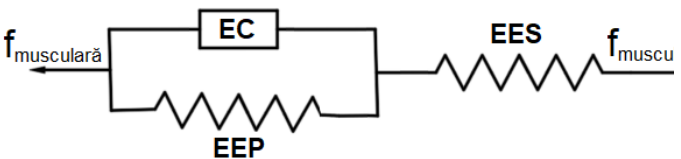
$$f_{\text{musculară}} = f_m = f_{EC} + f_{EEP} = f_{EES} \quad (4.7)$$


Figure 4. 30. The phenomenological model used to determine muscle activity.

The force developed by the contractile element can be determined by equation 4.8,

$$f_{EC}(F_{max}, a, l_{EC}, v_{EC}) = F_{max} \cdot a(t) \cdot f(l_{EC}) \cdot f(v_{EC}) \quad (4.8)$$

$$f(l_{EC}) = \exp\left(c \left| \frac{l_{EC} + l_{opt}}{wl_{opt}} \right|^3\right) \quad (4.9)$$

According to Figure 4.31, by increasing the length of the muscle fibre (contractile element), the active force generated by the skeletal muscle will increase to a maximum value

Chapter 4. Dynamic modelling of the human upper limb

called maximal isometric force. This corresponds to the optimal length of the contractile element, after which it decreases. According to the resulting data, it can be observed that the force decreases with exceeding the optimal length.

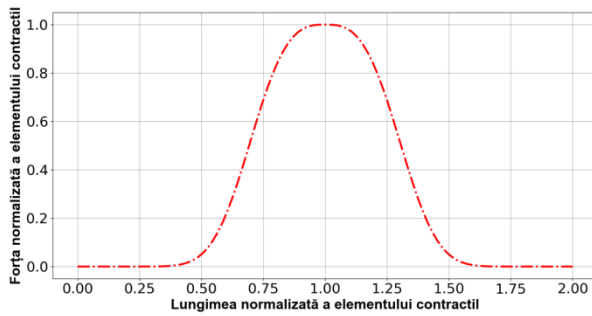


Figure 4. 31. Dependence between the force and the length of the contractile element.

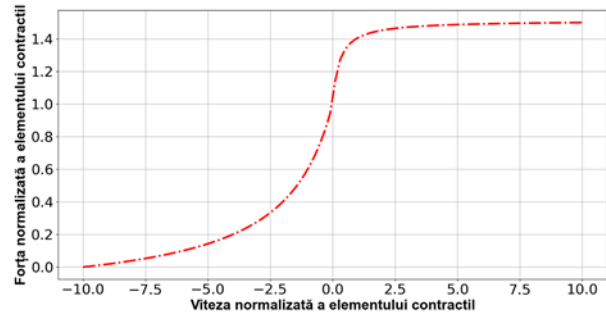


Figure 4. 32. Dependence between force and speed of the contractile element.

$$f(v_{EC}) = \begin{cases} 0, & v_{EC} \leq -1 \\ \frac{1 + v_{EC}}{1 - \frac{v_{EC}}{0,25}}, & -1 < v_{EC} \leq 0 \\ \frac{1 + 1,6 \cdot \frac{v_{EC}}{0,06}}{1 + \frac{v_{EC}}{0,06}}, & v_{EC} > 0 \end{cases} \quad (4.10)$$

According to figure 4.32, the muscle generates a force greater than the isometric maximum (corresponding to $v_{EC} = 0$) when it elongates, with an asymptotic behaviour, and a lower force until it reaches the maximum contraction speed v_{max} , beyond which it does not is still capable of producing force.

The muscle-tendon anatomical system is composed of a contractile element and an elastic one. The two elements are positioned in series. The force developed by the contractile element is dependent on the muscle activation state $a(t) \in [0,1]$, on the maximum isometric force (F_{max}), but also on the force-length ($f(l_{EC})$) and force-velocity ($f(v_{EC})$) (equation 4.8).

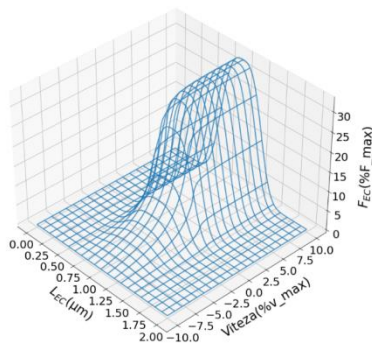


Figure 4. 33. Contractile element force as a function of skeletal muscle length and velocity for a given activation level, 3D representation

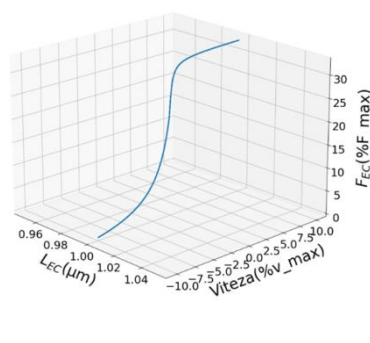


Figure 4. 34 Section of figure 4.11 for a constant length. This section suggests that for a constant length (1 μm), the curve described is the velocity-stress curve measured at that constant length, 1 μm .

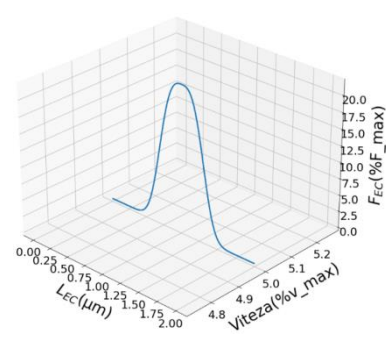


Figure 4. 35. Section of figure 4.11 for a constant speed. This section suggests that for an arbitrarily chosen constant velocity (5 m/s), the curve described is the length-tension curve measured at that velocity.

The EES elemen is characterized by a non-linear relationship between elastic force and length (equation 4.11) (van Ingen Schenau, 1984). The mechanical properties of human tendons are fairly well-known (Benedict et al., 1968; Blanton & Biggs, 1970). In the case of

Chapter 4. Dynamic modelling of the human upper limb

the Achilles tendon, the allowable tensile strength is reported to be in the range of 4000-6000N, and the relative elongation distance of 5-8%.

$$f_{EES}(l_{EES}) = \begin{cases} \left(\frac{l_{EES} - l_r}{0,04l_r^2} \right)^2, & \frac{l_{EES} - l_r}{l_r} > 0 \\ 0, & \frac{l_{EES} - l_r}{l_r} \leq 0 \end{cases} \quad (4.11)$$

Table 4. 6. Python code snippet for the function f_{EES} .

```
def forta_EES(l_EES):
    if (l_EES-l_r)/2 > 0.0:
        f_EES = ((l_EES-l_r)/(0.04*l_r**2.0))**2.0
        return f_EES
    else:
        return 0.0
l_EES = np.linspace(0, 1, 100)
forta_EES = np.vectorize(forta_EES)
F_EES = forta_EES(l_EES)
```

The force developed by the muscle-tendon complex is dependent on the tensions developed in the connective tissue, muscle fibre and tendon. According to a 2014 study (Buhrmann & Di Paolo, 2014), muscle strength can be determined with the following equation: $F = f_{EC}(F_{max}, a, l_{EC}, v_{EC}) + F_{max} \cdot f_{EES}(l_{EES})$ (4.12)

4.5. Phenomenological algorithm for the analysis of the biceps short end muscle

The study of the mechanical behaviour of skeletal muscle is one of the most approached studies in the field of biomechanics of the human body. Inverse and forward dynamic analyses are classic problems that require the description of muscle mechanical properties (Romero & Alonso, 2016).

In this subchapter, we analyzed the behaviour of the short-end biceps skeletal muscle through the lens of a phenomenological algorithm that we developed by combining two procedures specific to applied mechanics. In this sense, the developed algorithm presents a combination of the method of homogeneous rotation transformations with the model described by Archibald Vivian Hill.

The mathematical model described by the method of homogeneous rotation transformations aims to determine the kinematics of the biceps short-end muscle.

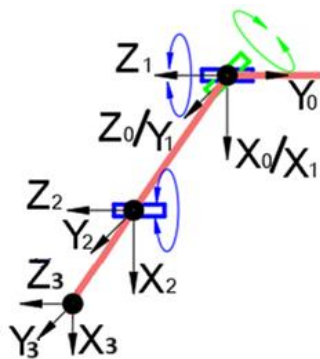


Figure 4. 36. Graphical representation of the coordinate systems associated with the 3-degree-of-freedom kinematic model couplings of the human arm and the effector positioned at the insertion site.

In Figure 4.36, the joints represented in blue allow flexion-extension movements, and the one in green abduction-adduction. For this study, we considered as input data for the simulation, values in correspondence with those from the norms presented previously, but also from the finite element analysis subchapter. Determining the mathematical model involves following successive stages (M. Novetschi et al., 2023). In the first stage, we established the kinematic elements (bones of the upper limb) associated with the studied kinematic chain, as well as the links between them.

Chapter 4. Dynamic modelling of the human upper limb

Următoarea etapă este determinarea sistemului de coordonate pentru prima cuplă. În acest sens am ales axa z_0 ca axă de rotație. Orientarea celorlalte două axe este în corespondență cu regula mâinii drepte.

Matricele de transformare omogenă de rotație sunt compuse din ecuația de rotație (R_i^{i-1}) a sistemului $O_i x_i y_i z_i$ față de sistemul $O_{i-1} x_{i-1} y_{i-1} z_{i-1}$, matricea de orientare (I_i^{i-1}), dar și de vectorul de deplasare (d_i^{i-1}).

The next step is to determine the coordinate system for the first couple. In this sense, we chose the z_0 axis as the axis of rotation. The orientation of the other two axes is in correspondence with the right-hand rule.

The homogeneous rotation transformation matrices are composed of the rotation equation (R_i^{i-1}) of the $O_i x_i y_i z_i$ system with respect to the $O_{i-1} x_{i-1} y_{i-1} z_{i-1}$ system, the orientation matrix (I_i^{i-1}), but also by the displacement vector (d_i^{i-1}).

$$H_1^0 = \begin{bmatrix} R_1^0 & d_1^0 \\ 0 & 0 & 0 & 1 \end{bmatrix} = \begin{bmatrix} \cos\theta_1 & 0 & \sin\theta_1 & 0 \\ \sin\theta_1 & 0 & -\cos\theta_1 & 0 \\ 0 & 1 & 0 & 0 \\ 0 & 0 & 0 & 1 \end{bmatrix} \quad (4.13)$$

$$H_2^1 = \begin{bmatrix} R_2^1 & d_2^1 \\ 0 & 0 & 0 & 1 \end{bmatrix} = \begin{bmatrix} \cos\theta_2 & 0 & -\sin\theta_2 & l_h \cdot \cos\theta_2 \\ \sin\theta_2 & 0 & \cos\theta_2 & l_h \cdot \sin\theta_2 \\ 0 & 1 & 0 & 0 \\ 0 & 0 & 0 & 1 \end{bmatrix} \quad (4.14)$$

$$H_3^2 = \begin{bmatrix} R_3^2 & d_3^2 \\ 0 & 0 & 0 & 1 \end{bmatrix} = \begin{bmatrix} \cos\theta_3 & 0 & -\sin\theta_3 & l_i \cdot \cos\theta_3 \\ \sin\theta_3 & 0 & \cos\theta_3 & l_i \cdot \sin\theta_3 \\ 0 & -1 & 0 & 0 \\ 0 & 0 & 0 & 1 \end{bmatrix} \quad (4.15)$$

$$H_3^0 = \prod_{i=0}^3 H_i^{i-1} = \begin{bmatrix} \cos\theta_1 & 0 & \sin\theta_1 & 0 \\ \sin\theta_1 & 0 & -\cos\theta_1 & 0 \\ 0 & 1 & 0 & 0 \\ 0 & 0 & 0 & 1 \end{bmatrix} \cdot \begin{bmatrix} \cos\theta_2 & 0 & -\sin\theta_2 & l_h \cdot \cos\theta_2 \\ \sin\theta_2 & 0 & \cos\theta_2 & l_h \cdot \sin\theta_2 \\ 0 & 1 & 0 & 0 \\ 0 & 0 & 0 & 1 \end{bmatrix} \cdot \begin{bmatrix} \cos\theta_3 & 0 & -\sin\theta_3 & l_i \cdot \cos\theta_3 \\ \sin\theta_3 & 0 & \cos\theta_3 & l_i \cdot \sin\theta_3 \\ 0 & -1 & 0 & 0 \\ 0 & 0 & 0 & 1 \end{bmatrix} \quad (4.16)$$

Figure 4.37 contains a comparative analysis between the variation of muscle length and speed in the studied time interval. These developments are characteristic of concentric-isotonic contraction and are supported by the literature. The data resulting from this graph are input data for the second component of the phenomenological algorithm, more specifically Archibald Vivian Hill's model.

To describe the force developed by the contractile element of the short-end biceps muscle, it is necessary to determine the relationship between force and length (figure 4.38) and also that between force and speed (figure 4.39). These dependencies have as input data the variables shown in figure 4.37. More precisely, Hill's model requires knowledge of the kinematics of the analyzed skeletal muscle.

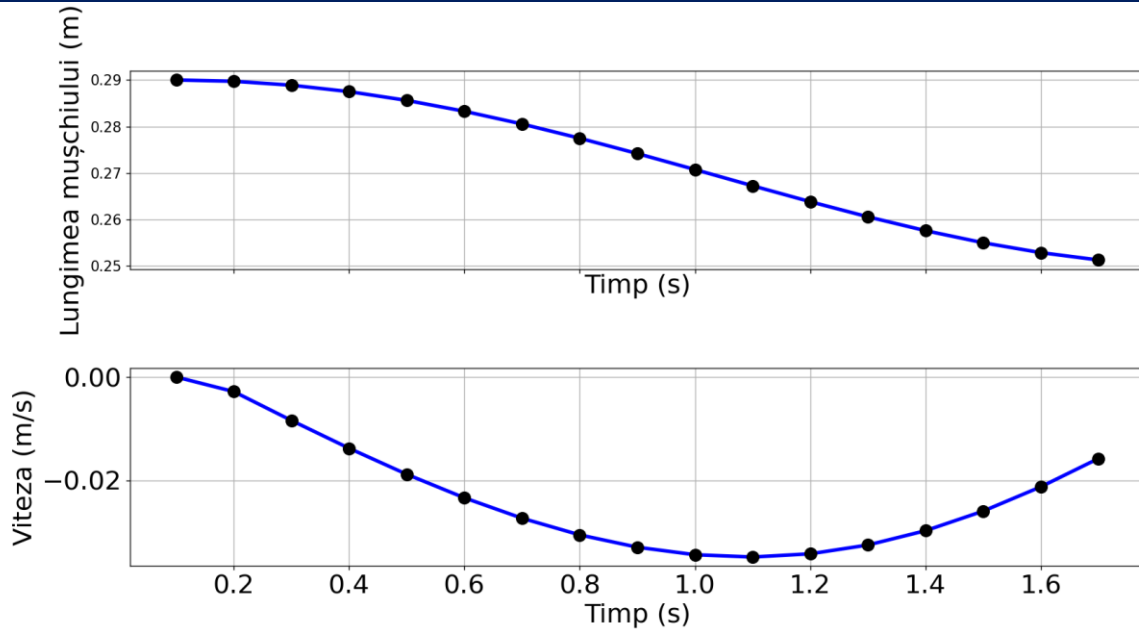


Figure 4. 37. Comparative analysis between the variation of muscle length and speed in the studied time interval.

. The graphic representation of the two dependencies is rendered according to the variation of the angle $\theta_3 \in [0^\circ; 160^\circ]$. In this case, the other two angles (θ_1 and θ_2) are not taken into account, because their variation does not change the length of the muscle fiber. The angles in question were introduced for future research directions.

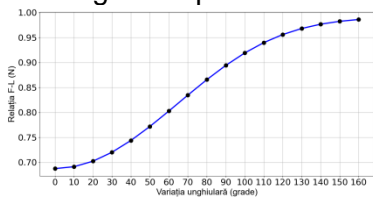


Figure 4. 38. Dependence between the force-length (F-L) relationship and the variation of the angle of rotation of the coupling in the elbow.

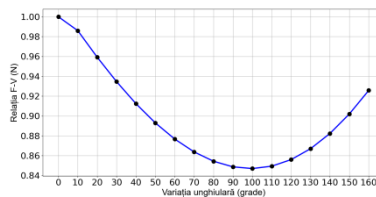


Figure 4. 39. The dependence of the force-velocity (F-V) relationship and the variation of the angle of rotation of the coupling in the elbow.

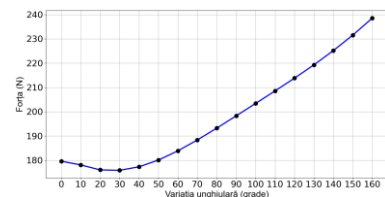


Figure 4. 40. The variation of the force developed by the contractile element with the variation of the rotation angle of the coupling in the elbow.

Figure 4.40 shows the evolution of the force developed by the contractile element for the short-end biceps muscle. In this case, the force is dependent on the force-length and force-velocity relationships, but also on the maximum isometric force. This is a constant that in this study we set as the maximum value described by the biceps brevis muscle in the finite element analysis.

Comparing figure 4.40 with 4.26 it can be seen that the two developments are similar. Muscle force decreases at the beginning of both simulations followed by a sustained increase throughout the elbow flexion angle variation.

4.6. Pseudocode algorithm for phenomenological analysis of skeletal muscle

This chapter contains a sequence of calculation steps aimed at determining the force developed by the biceps brevis skeletal muscle. The steps of this algorithm are:

- The pseudocode for the mathematical model that reflects the positional analysis of the effector through homogeneous rotation transformations.
- The pseudocode for the model developed by Archibald Vivian Hill describing muscle contraction of skeletal muscle.

Algorithm 3. Phenomenological analysis of the biceps short end skeletal muscle	
1	$(x_3^0, y_3^0, z_3^0) \leftarrow$ "defining null vectors"
2	$(0, 0, 0, 1) \leftarrow$ "complement vector definition"
3	number of analyzed positions, humerus length, insertion distance \leftarrow user input
4	human_upper_limb_3DoF \leftarrow function definition
5	$(\theta_1, \theta_2, \theta_3) \leftarrow$ user input
6	# defining the 2 degrees of freedom associated with the shoulder joint
7	# define flexion-extension movement
8	$(r_1^0, l_1^0, d_1^0) \leftarrow$ define matrix and vector components
9	$(r_1^0, l_1^0) \leftarrow R_1^0$
10	$(R_1^0, d_1^0) \leftarrow H_1^0$
11	# adduction abduction movement definition
12	$(r_2^1, l_2^1, d_2^1) \leftarrow$ define matrix and vector components
13	$(r_2^1, l_2^1) \leftarrow R_2^1$
14	$(R_2^1, d_2^1) \leftarrow H_2^1$
15	# defining the degree of freedom associated with the elbow joint – flexion – extension movement
16	$(r_3^2, l_3^2, d_3^2) \leftarrow$ define matrix and vector components
17	$(r_3^2, l_3^2) \leftarrow R_3^2$
18	$(R_3^2, d_3^2) \leftarrow H_3^2$
32	$\prod_{i=0}^3 H_i^{i-1} \leftarrow H_3^0$
33	$(x_3^0, y_3^0, z_3^0) \leftarrow$ return
34	for $i \in [0, \text{număr de poziții}]$ do
35	human_lower_limb_3DoF
36	$(x_3^0, y_3^0, z_3^0) \leftarrow$ print
37	$(x_3^0, y_3^0, z_3^0) \rightarrow l_{EC} \leftarrow$ plot the length of the contractile element
38	$l_{EC} \rightarrow v_{EC} \leftarrow$ plot the shortening speed of the contractile element
39	$l_{EC} \rightarrow f(l_{EC}) \leftarrow$ plot force - length relationship
40	$v_{EC} \rightarrow f(v_{EC}) \& \leftarrow$ plot force - speed relationship
41	$f(v_{EC}) \& f(l_{EC}) \rightarrow f_{EC} \leftarrow$ plot the force relationship developed by the contractile element

4.7. Conclusions

The present chapter, entitled Dynamic Modelling of the human upper limb, contains an analysis of the mechanical behaviour of the biceps muscle, but especially of its shorter component, the biceps brevis.

In this chapter we analyzed through the prism of methods (techniques) specific to applied mechanics, the force developed by the muscular structure presented previously, depending on the variation of the flexion angle in the elbow.

The first method approached is that of finite elements (FEM), from where we extracted the forces developed by the two muscle components, the total moment, and also the deformation produced. What is worth noting is that the two muscles apparently act in opposition. At the same time, based on the numerical data, we applied the polynomial regression method to determine the mathematical models that describe mechanical behaviour. We thus obtained polynomial functions of higher order. However, given the high degree of these polynomials, they may be characterized by over-adaptability.

Chapter 4. Dynamic modelling of the human upper limb

Another aspect addressed in this chapter is the kinematic study of the biceps short-end skeletal muscle. Using the method of homogeneous rotation transformations, we determined the position in the tri-orthogonal space of the muscle insertion point. Knowing the coordinates in time and space, I deduced the variation of the length of the muscle and implicitly of the speed of shortening. The data results are confirmed by studies in the field regarding the specific behaviour of a concentric contraction. We further used these data as input data for the phenomenological algorithm. From the analysis of the resulting data, it can be concluded that both the finite element analysis and the numerical results from the created script denote the same variability for the muscle force developed by the short-end biceps muscle.

CHAPTER 5.

GENERAL CONCLUSIONS OF THE MATHEMATICAL MODELING OF THE HUMAN MECHANICAL SYSTEM

5.1. General conclusions

The architecture and analysis of the biomechanical system of the human body highlighted the objectives of the doctoral thesis, namely the development of theoretical computer models of the movements of the human body. The principles of modelling biomechanical systems highlighted the various techniques and models used in this field of research, using functional models, which highlight components and interactions to result in system functions, or theoretical models, based on which phenomena are described, both qualitatively and quantitatively.

The estimation of anthropometric parameters can be done by direct measurements, mathematical modelling or medical imaging techniques. Modern approaches integrate mathematical models and imaging technologies to obtain the most accurate estimates of anthropometric parameters. Such data are fundamental in the design of personalized medical devices and in optimizing the performance of athletes.

The advantages of mathematical modelling stand out, especially in the case of complex biomechanical systems when it is necessary to determine a series of parameters using non-invasive methods. Thus, the investigation of a particular subsystem is possible when actual experiments cannot be performed. At the same time, the use of the model allows iterating on various anthropometrics as many times as needed to achieve a more accurate analysis. Also, by changing the parameters of the biomechanical system, the extreme values of the variables can be established, values that would correspond to anatomical limit positions. We can conclude that the study based on models is much more effective both qualitatively and economically (low costs, reduced time, etc.)

The head-neck-spine analytical model can be used when the angular variations of the studied anatomical elements (θ_1 , θ_2 , θ_3) can be determined. This is possible with a series of computer applications that use markers (Kinovea) or with the help of sensors that can determine angular displacements. The developed model can determine the values of the forces responsible for the movement of the head, neck or trunk, but also the restorative forces responsible for returning the body to the orthostatic position.

Based on the developed mathematical model, a computer application was created to determine the values of the disturbing forces responsible for removing the analyzed system from the equilibrium position. The model thus developed was validated using real data and observations to ensure relevance and similarity to real situations that present a risk of injury. The validation was done with the help of a neural network. Comparing the RNA results with the mathematical model leads to the conclusion that the neural model predicts the muscle forces quite accurately, thus validating the mathematical model. Using the model allows iterating on various anthropometrics as many times as needed to get a more accurate analysis. In addition, any change in the parameters of the biomechanical system can provide the extreme values of the variables that correspond to the anatomical limit positions.

Chapter 5. General conclusions of the mathematical modeling of the human mechanical system

Network test results can be compared with performance on validation data to determine network effectiveness. The accuracy of neural network predictions depends on several factors, such as the quality of the training data, the size and architecture of the neural network, the training algorithm, and its parameters. The presented neural model has a very good performance with an error of up to 2.633%. However, improving model performance requires collecting additional anthropometric data from various typologies and adjusting the model architecture or other aspects of the training process.

Assessing the performance and generalizability of the mathematical model is essential in providing confidence that the mathematical model is robust and can make accurate predictions on new data. The use of neural networks to validate mathematical models is an effective method in certain situations. Validating a mathematical model using neural networks requires a deep understanding of the problem and the mathematics involved, as well as the proper use and interpretation of neural network tools.

Therefore, data testing using a neural network is a crucial step in the process of RNA model development and evaluation and plays an important role in the generalization of the prediction model. Easy NN software allows exporting the trained neural model for use with other applications or integration into other systems, providing an advantage.

For the dynamic modelling of the human upper limb, we analyzed the mechanical behaviour of the biceps muscle, especially its shorter component, the biceps short end. The analysis of the muscular force developed by the short-end biceps structure was carried out through the prism of specific methods applied to the mechanics, depending on the variation of the elbow flexion angle.

The first method approached is the finite element method (FEM), from where we extracted the forces developed by the two muscle components, the total moment, and also the deformation produced. What is worth noting is that the two muscles apparently act in opposition. At the same time, based on the numerical data, we applied the polynomial regression method to determine the mathematical models that describe mechanical behaviour. We thus obtained polynomial functions of higher order. However, given the high degree of these polynomials, they may be characterized by over-adaptability. Overfitting can occur when a model, such as a polynomial function, is too complex for the available data, and the model tries to adjust for noise or random variability in the training data instead of identifying real relationships in the data. This can lead to poor model performance on new, unknown data. To avoid overfitting, it is important to choose an appropriate degree of polynomial and use regularization techniques to control the complexity of the model. As a future direction, I propose to test these technical optimization models and adapt them to be generalizable.

Another aspect addressed in the chapter on dynamic modelling of the human upper limb was the kinematic study of the biceps brevis skeletal muscle. Using the method of homogeneous rotation transformations, we determined the position in the tri-orthogonal space of the muscle insertion point. Knowing the coordinates in time and space, I deduced the variation of the length of the muscle and implicitly of the speed of shortening. The data results are confirmed by studies in the field regarding the specific behaviour of a concentric contraction. We further used these data as input data for the phenomenological algorithm. From the analysis of the resulting data, it can be concluded that both the finite element analysis and the numerical results from the created script denote the same variability for the muscle force developed by the short-end biceps muscle.

In this doctoral thesis, I used a new approach in the field of biomechanics, namely that of homogeneous rotation transformations, an approach mainly used in the study of manipulators and robots. This method involves determining the rotation matrix and displacement vector for each studied joint (movement) relative to the reference joint (global reference system $O_0x_0y_0z_0$). The direct result is represented by the scalar components of the displacement vector described by the end effector. The end effector is the theoretical point located at the tip of the toes or fingers.

Chapter 5. General conclusions of the mathematical modeling of the human mechanical system

The movement of the segments of the human body, regardless of the analyzed kinematic chain, is a complex one. Human kinematic chains (lower limbs, upper limbs, trunk or whole body) can perform planar or spatial movements. However, rarely are the movements produced by kinematic chains exclusively planar. In this case, planar movements can only be considered if the goal is to simulate certain movements, such as flexion and extension or abduction and adduction. To be able to analyze the movement of the human body as a whole or a part, mathematical models or multi-body models can be used. Mathematical models in this PhD thesis can be adapted so that the degree of complexity increases or decreases.

Thus, planar or spatial movements can be simulated. By blocking the described movements of the kinematic chains, movements of the kinematic chains from one degree of freedom up to 6 degrees of freedom can be simulated. To increase the complexity of the models (over 6 degrees of freedom) they can be easily adjusted by adding the homogeneous matrices associated with the desired movements to be analyzed. The maximum complexity to which these models can be adjusted without considering phalanx joints is 10 DoF. The 10 degrees of freedom involve the analysis of the main movements executed by the upper or lower kinematic chains.

Mathematical models were developed using the Python programming language, a fast and efficient programming language used by researchers around the world to develop cutting-edge solutions, and simulation was performed for all 6 cases studied, 10 positions each.

5.2. Personal contributions

In the framework of this doctoral thesis, I believe that I have made a series of original personal contributions that can be the precursors of future studies in the field of mathematical modelling of the human mechanical system. The main personal contributions to the doctoral thesis are as follows:

1. Development and application of a mathematical model that has demonstrated its efficiency and utility in determining critical parameters using non-invasive methods, in the context of investigating complex biomechanical systems,
2. Highlighting the fact that mathematical modelling offers significant advantages in situations where real experiments are not feasible or are limited.
3. Through the head-neck-spine mathematical model, we investigated and analyzed the specific subsystems without the need for invasive or expensive experiments, considering that this subsystem works as a triple inverted pendulum.
4. We also extended the model to evaluate the forces responsible for head, neck and trunk movements, as well as the restorative forces responsible for returning the body to the orthostatic position. This detailed analysis allowed me to better understand the biomechanics of the upper body and identify the factors that influence these movements.
5. We performed a parameterized analysis of the model we proposed to determine the values of the disruptive and/or restorative forces according to various anthropometrics.
6. I developed a computer application in the C++ programming language for the value determination of the disturbing forces, with the help of which I provided these values according to different anthropometrics.
7. We validated the mathematical model of the biomechanics of the head, neck and spine with the help of neural networks, this validation represents an important and even innovative contribution to the field of biomechanics. By integrating neural networks in the model validation process, we obtained a deeper and more detailed understanding of the behaviour of these biomechanical subsystems, concluding that at their level a series of forces develop whose value can be compared to the values of the impact forces at which the human body is subject.
8. I used the experimental data or determined with the help of C++ application to train the neural network to recognize and validate the proposed model for the biomechanics of the

Chapter 5. General conclusions of the mathematical modeling of the human mechanical system

head, neck and spine. The main contribution of this process lies in the ability of neural networks to learn and identify complex and non-linear patterns in the input data.

9. I created a complex, but also adaptive mathematical model (translated into the Python programming environment), for the kinematic analysis of the human upper limb. This model is based on the method of homogeneous rotation transformations, a method used mainly in robotics. With the help of this script, we analyzed the spatial displacement of the human upper limb. I note that the model can vary in complexity by adding new rotation matrices or by cancelling homogeneous rotation transformations desired for particular studies.
10. I performed the positional analysis of the human lower limb by the method of homogeneous rotation transformations. In this regard, we created a mathematical model transposed in the Python programming language for the analysis of the spatial movement of the kinematic chain of the human lower limb. The mathematical model simulates a kinematic chain with a maximum of 6 degrees of freedom that can vary in complexity depending on the desired analysis.
11. I analyzed the mechanical behaviour of the biceps muscle (the components biceps short end and biceps long end) and implicitly the effect it has on the deformation of the arm-forearm mechanical system. From this analysis, we deduced the maximum force developed by the short-end biceps muscle, necessary for the phenomenological algorithm;
12. I mathematically modeled the mechanical behavior of the biceps muscle using the higher-order polynomial regression method;
13. I developed a phenomenological algorithm for the analysis of the biceps short-end skeletal muscle. A phenomenological mathematical algorithm is a type of mathematical modelling that aims to describe and predict observed phenomena without necessarily exploring the underlying mechanisms of the analyzed process. I have translated the algorithm into the Python programming environment and it contains the mathematical model of muscle force variation created by Archibald Vivian Hill, but also a mathematical model that I created and which aims to determine the kinematics of the biceps brevis skeletal muscle. The latter model we created using the method of homogeneous transformations and it generates the input data needed to train the Hill model.

5.3. Future research directions

This PhD thesis opens up several new research opportunities from a kinematic and dynamic point of view regarding the biomechanics of the human body. Thus, I propose the following:

1. Adaptation and application of the analytical head-neck-spine model for the whole human body in the orthostatic position to determine the angular variations of all anatomical elements. This can be achieved using specialized computer applications that use markers or sensors to measure angular displacements. This approach will allow me to adjust and optimize the model to more accurately reflect individual variations in biomechanical parameters, which will contribute to a more accurate analysis of the force values developed by the muscle groups responsible for maintaining the human body in a certain position.
2. I also propose an optimization of the forces developed by the driver's muscle groups in the event of a frontal impact by sizing the seat belt tension as accurately as possible.
3. I will continue to use neural networks for seat belt sizing. Based on the collected data I will train these neural networks to learn the complex relationships between vehicle parameters, impact and seat belt tension. Once trained, the neural networks will be able to be used to estimate the optimal tensions in the seat belts in various scenarios and conditions so that the muscle groups develop forces accessible to the human body that do not cause muscle damage.

Chapter 5. General conclusions of the mathematical modeling of the human mechanical system

4. By integrating neural networks into the seat belt sizing process, I aim to develop more efficient and safer seat belts that provide optimal protection in the event of a road accident. This process can also help me to identify and eliminate potential deficiencies or design issues in existing seat belts, which can help improve vehicle safety and reduce the risk of direct or indirect injury (muscle strains, ligament tears or muscles) in road accidents.
5. Mathematical modelling by the method of homogeneous rotational transformations of the entire human body and of various kinematic chains specific to particular activities and actions;
6. Creation of a more complex phenomenological algorithm from the point of view of the considered biological elements. More precisely, I propose the introduction in this algorithm of the other component elements associated with the skeletal muscle (elements placed in series and parallel);
7. Finite element modelling of a more complex mechanical system in terms of the number of muscles and kinematic elements;
8. Testing the mathematical models described by the higher order polynomial regression method to determine if they are over-adaptable to the generated experimental data;
9. Extension of the phenomenological algorithm for more complex particular analyses. Thus, I want to be able to simulate not only the behaviour of the agonist muscle (responsible for direct action) but also of the antagonist muscle (responsible for breaking direct action) through this algorithm.

SELECTIVE BIBLIOGRAPHY

1. Alizadeh, M., Knapik, G. G., Mageswaran, P., Mendel, E., Bourekas, E., & Marras, W. S. (2020). Biomechanical musculoskeletal models of the cervical spine: A systematic literature review. *Clinical Biomechanics*, 71, 115–124. <https://doi.org/10.1016/j.clinbiomech.2019.10.027>
2. Amortila, V., Mereuta, E., Novetschi, M., Rus, M., & Vereşiu, S. (2021). ANALYTIC MODEL OF THE SUBSYSTEM HEAD-NECK-SPINE MOVEMENT BIOMECHANICS. *Mechanical Testing and Diagnosis*, 11(1), Article 1. <https://doi.org/10.35219/mtd.2021.1.03>
3. Arslan, Y. Z., Karabulut, D., Ortes, F., & Popovic, M. B. (2019). 11 - Exoskeletons, Exomusculatures, Exosuits: Dynamic Modeling and Simulation. In M. B. Popovic (Ed.), *Biomechatronics* (pp. 305–331). Academic Press. <https://doi.org/10.1016/B978-0-12-812939-5.00011-2>
4. Bahadori, S., & Wainwright, T. W. (2020). Lower Limb Biomechanical Analysis of Healthy Participants. *JOVE-JOURNAL OF VISUALIZED EXPERIMENTS*, 158, e60720. <https://doi.org/10.3791/60720>
5. Bajd, T., Mihelj, M., Lenarčič, J., Stanovnik, A., & Munih, M. (2010). Homogenous transformation matrices. In T. Bajd, M. Mihelj, J. Lenarcic, A. Stanovnik, & M. Munih (Eds.), *Robotics* (pp. 9–22). Springer Netherlands. https://doi.org/10.1007/978-90-481-3776-3_2
6. Benedict, J. V., Walker, L. B., & Harris, E. H. (1968). Stress-strain characteristics and tensile strength of unembalmed human tendon. *Journal of Biomechanics*, 1(1), 53–63. [https://doi.org/10.1016/0021-9290\(68\)90038-9](https://doi.org/10.1016/0021-9290(68)90038-9)
7. Bjørnstrup, J. (1995). Estimation of human body segment parameters: Historical background. In *Estimation of human body segment parameters* [Report]. Aalborg University, Laboratory of Image Analysis.
8. Blanton, P. L., & Biggs, N. L. (1970). Ultimate tensile strength of fetal and adult human tendons. *Journal of Biomechanics*, 3(2), 181–189. [https://doi.org/10.1016/0021-9290\(70\)90005-9](https://doi.org/10.1016/0021-9290(70)90005-9)
9. Brahmi, B., Laraki, M. H., Saad, M., Rahman, M. H., Ochoa-Luna, C., & Brahmi, A. (2019). Compliant adaptive control of human upper-limb exoskeleton robot with unknown dynamics based on a Modified Function Approximation Technique (MFAT). *Robotics and Autonomous Systems*, 117, 92–102. <https://doi.org/10.1016/j.robot.2019.02.017>
10. Buhrmann, T., & Di Paolo, E. A. (2014). Spinal circuits can accommodate interaction torques during multijoint limb movements. *Frontiers in Computational Neuroscience*, 8, 144. <https://doi.org/10.3389/fncom.2014.00144>
11. Cardona, M., & Garcia Cena, C. E. (2019). Biomechanical Analysis of the Lower Limb: A Full-Body Musculoskeletal Model for Muscle-Driven Simulation. *IEEE Access*, 7, 92709–92723. <https://doi.org/10.1109/ACCESS.2019.2927515>
12. Chen, R., Yuan, Y., & Thomson, D. (2021). A review of mathematical modelling techniques for advanced rotorcraft configurations. *Progress in Aerospace Sciences*, 120, 100681. <https://doi.org/10.1016/j.paerosci.2020.100681>
13. De Jager, M., Sauren, A., Thunnissen, J., & Wismans, J. (1996). *A Global and a Detailed Mathematical Model for Head-Neck Dynamics*. 962430. <https://doi.org/10.4271/962430>
14. Dereshgi, H. (2023). Investigating the biomechanics of the biceps brachii muscle during dumbbell curl exercise: A comprehensive approach. *European Mechanical Science*, 7, 209–219. <https://doi.org/10.26701/ems.1348070>

Selective bibliography

15. Dou, R., Yu, S., Li, W., Chen, P., Xia, P., Zhai, F., Yokoi, H., & Jiang, Y. (2022). Inverse kinematics for a 7-DOF humanoid robotic arm with joint limit and end pose coupling. *Mechanism and Machine Theory*, 169, 104637. <https://doi.org/10.1016/j.mechmachtheory.2021.104637>
16. Drăgulescu, D. (2005). *Modelare în biomecanică*. Editura Didactică și Pedagogică.
17. GHERASIM, D. M., & ARGHIR, M. (2021). STUDY OF THE FREE VIBRATIONS OVER THE MUSCULAR SYSTEM OF THE HUMAN BODY. PART I: MECHANICAL CHARACTERISTICS OF THE LEFT DELTOID. *ACTA TECHNICA NAPOCENSIS - Series: APPLIED MATHEMATICS, MECHANICS, and ENGINEERING*, 64(1). <https://atna-mam.utcluj.ro/index.php/Acta/article/view/1562>
18. Gillawat, A. K. (2022). Development of a revolute-type kinematic model for human upper limb using a matrix approach. *ROBOTICA*, 40(6), 1833–1854. <https://doi.org/10.1017/S0263574721001387>
19. Gismelseed, S., Al-Yahmedi, A., & Zaier, R. (2023). A biped model to predict a wide range of gait and posture results. *Franklin Open*, 3, 100020. <https://doi.org/10.1016/j.fraope.2023.100020>
20. Hanavan, J., & Ernest, P. (1964). *A mathematical model of the human body*. <https://apps.dtic.mil/sti/citations/AD0608463>
21. Hart, N. H., Nimphius, S., Rantalainen, T., Ireland, A., Siafarikas, A., & Newton, R. U. (2017). Mechanical basis of bone strength: Influence of bone material, bone structure and muscle action. *Journal of Musculoskeletal & Neuronal Interactions*, 17(3), 114–139.
22. Hatze, H. (1976). The complete optimization of a human motion. *Mathematical Biosciences*, 28(1), 99–135. [https://doi.org/10.1016/0025-5564\(76\)90098-5](https://doi.org/10.1016/0025-5564(76)90098-5)
23. He, W., He, K., Cui, H., & Wang, G. (2022). Using a rhythmic human shaker to identify modal properties of a stationary human body on a footbridge. *Journal of Sound and Vibration*, 540, 117309. <https://doi.org/10.1016/j.jsv.2022.117309>
24. Huang, Z., Pu, X., Tang, G., Ping, M., Jiang, G., Wang, M., Wei, X., & Ren, Y. (2022). BS-80K: The first large open-access dataset of bone scan images. *Computers in Biology and Medicine*, 151, 106221. <https://doi.org/10.1016/j.combiomed.2022.106221>
25. Huxley, A. F. (1957a). 6—Muscle Structure and Theories of Contraction. *Progress in Biophysics and Biophysical Chemistry*, 7, 255–318. [https://doi.org/10.1016/S0096-4174\(18\)30128-8](https://doi.org/10.1016/S0096-4174(18)30128-8)
26. Huxley, A. F. (1957b). Muscle structure and theories of contraction. *Progress in Biophysics and Biophysical Chemistry*, 7, 255–318.
27. Islas, J. C. G., Domínguez-Ramírez, O. A., & Ortega, O. L. (2020). Biped Gait Analysis based on Forward Kinematics Modeling using Quaternions Algebra. *Mexican Journal of Biomedical Engineering*, 41(3), Article 3.
28. Jaimes, W. J., Mantilla, J. F., Salinas, S. A., & Navarro, H. J. (2021). Modeling and Simulation of a Lower Limb Exoskeleton with Computed Torque Control for Gait Rehabilitation. In L. L. Salas & R. Leder (Eds.), *2021 GLOBAL MEDICAL ENGINEERING PHYSICS EXCHANGES/PAN AMERICAN HEALTH CARE EXCHANGES (GMEPE/PAHCE)*. IEEE. <https://doi.org/10.1109/GMEPE/PAHCE50215.2021.9434854>
29. Jiang, H., Diao, Z., Shi, T., Zhou, Y., Wang, F., Hu, W., Zhu, X., Luo, S., Tong, G., & Yao, Y.-D. (2023). A review of deep learning-based multiple-lesion recognition from medical images: Classification, detection and segmentation. *Computers in Biology and Medicine*, 157, 106726. <https://doi.org/10.1016/j.combiomed.2023.106726>
30. Kitade, I., Nakajima, H., Takahashi, A., Matsumura, M., Shimada, S., Kokubo, Y., & Matsumine, A. (2020). Kinematic, kinetic, and musculoskeletal modeling analysis of gait in patients with cervical myelopathy using a severity classification. *The Spine Journal*, 20(7), 1096–1105. <https://doi.org/10.1016/j.spinee.2020.01.014>
31. Klöpfer-Krämer, I., Brand, A., Wackerle, H., Müßig, J., Kröger, I., & Augat, P. (2020). Gait analysis – Available platforms for outcome assessment. *Injury*, 51, S90–S96. <https://doi.org/10.1016/j.injury.2019.11.011>

Selective bibliography

32. Kumar, N. R., & Y, R. K. (2023). Efficient medical image retrieval system using Geometric Invariant Point Bilateral Transformation (GIPBT). *Measurement: Sensors*, 27, 100705. <https://doi.org/10.1016/j.measen.2023.100705>
33. Lai, Y., Sutjipto, S., Carmichael, M. G., & Paul, G. (2021). Preliminary Validation of Upper Limb Musculoskeletal Model using Static Optimization. *2021 43RD ANNUAL INTERNATIONAL CONFERENCE OF THE IEEE ENGINEERING IN MEDICINE & BIOLOGY SOCIETY (EMBC)*, 4509–4512. <https://doi.org/10.1109/EMBC46164.2021.9629494>
34. Lechosa Urquijo, E., Blaya Haro, F., Cano-Moreno, J. D., D'Amato, R., & Juanes Méndez, J. A. (2022). Mechanical Model and FEM Simulations for Efforts on Biceps and Triceps Muscles under Vertical Load: Mathematical Formulation of Results. *Mathematics*, 10(14), Article 14. <https://doi.org/10.3390/math10142441>
35. Lutz, M. (2003). *Learning Python* (2nd ed.). O'Reilly & Associates, Inc.
36. Martínez, O., & Campa, R. (2021). Comparing Methods Using Homogeneous Transformation Matrices for Kinematics Modeling of Robot Manipulators. In M. Pucheta, A. Cardona, S. Preidikman, & R. Hecker (Eds.), *Multibody Mechatronic Systems* (pp. 110–118). Springer International Publishing.
37. Meyer, F., Humm, J., Yoganandan, N., Leszczynski, A., Bourdet, N., Deck, C., & Willinger, R. (2021). Development of a detailed human neck finite element model and injury risk curves under lateral impact. *Journal of the Mechanical Behavior of Biomedical Materials*, 116, 104318. <https://doi.org/10.1016/j.jmbbm.2021.104318>
38. Naaji, A. (2008). Dynamic modeling of the human upper limb. In D. Dimitrov, V. Mladenov, S. Jordanova, & N. Mastorakis (Eds.), *ADVANCED TOPICS ON EVOLUTIONARY COMPUTING* (pp. 98–101).
39. Nenciu, G. (2012). *BIOMECANICĂ Curs în tehnologia IFR*. Fundației „România de Măine”.
40. Nguyen, C., & Leonessa, A. (2014). *Control motion of a human arm: A simulation study* (p. 989).
41. Nguyen, K.-D., Chen, I.-M., Luo, Z., Yeo, S., & Duh, H. (2009). *A Body Sensor Network for Tracking and Monitoring of Functional Arm Motion* (p. 3867). <https://doi.org/10.1109/IROS.2009.5353912>
42. Novetschi, M. M., Mereuta, E., Nazer, T., Ganea, D., & Mereuta, C. (2023). Human upper limb positional analysis using homogenous transformation matrix. *BALNEO AND PRM RESEARCH JOURNAL*, 14(3), 567. <https://doi.org/10.12680/balneo.2023.567>
43. Novetschi, M., Mereuta, E., Nazer, T., Ganea, D., & Mereuta, C. (2023). Human upper limb positional analysis using homogenous transformation matrix. *Balneo and PRM Research Journal*, 14, 567. <https://doi.org/10.12680/balneo.2023.567>
44. Pecolt, S., Błażejowski, A., Królikowski, T., & Katafiasz, D. (2022). Multi-segment, spatial biomechanical model of a human body. *Procedia Computer Science*, 207, 272–281. <https://doi.org/10.1016/j.procs.2022.09.060>
45. Pennestri, E., Stefanelli, R., Valentini, P. P., & Vita, L. (2007). Virtual musculo-skeletal model for the biomechanical analysis of the upper limb. *JOURNAL OF BIOMECHANICS*, 40(6), 1350–1361. <https://doi.org/10.1016/j.jbiomech.2006.05.013>
46. Peyer, K. E., Morris, M., & Sellers, W. I. (2015). Subject-specific body segment parameter estimation using 3D photogrammetry with multiple cameras. *PeerJ*, 3, e831. <https://doi.org/10.7717/peerj.831>
47. Ramasamy, M. D., Dhanaraj, R. K., Pani, S. K., Das, R. P., Movassagh, A. A., Gheisari, M., Liu, Y., Porkar, P., & Banu, S. (2023). An improved deep convolutionary neural network for bone marrow cancer detection using image processing. *Informatics in Medicine Unlocked*, 38, 101233. <https://doi.org/10.1016/j.imu.2023.101233>
48. Robertson, E., Grace, S., Wallington, T., & Stewart, D. E. (2004). Antenatal risk factors for postpartum depression: A synthesis of recent literature. *General Hospital Psychiatry*, 26(4), 289–295. <https://doi.org/10.1016/j.genhosppsych.2004.02.006>

Selective bibliography

49. Romero, F., & Alonso, F. J. (2016). A comparison among different Hill-type contraction dynamics formulations for muscle force estimation. *Mechanical Sciences*, 7(1), 19–29. <https://doi.org/10.5194/ms-7-19-2016>
50. Roozbahani, H., Alizadeh, M., Ustinov, S., & Handroos, H. (2021). Development of a novel real-time simulation of human skeleton/muscles. *Journal of Biomechanics*, 114, 110157. <https://doi.org/10.1016/j.jbiomech.2020.110157>
51. Rusu, L., Toth-Tascau, M., & Toader-Pasti, C. (2014). Virtual Geometric Model of the Human Lower Limb. In L. Marsavina (Ed.), *PROCEEDINGS OF THE 14TH SYMPOSIUM ON EXPERIMENTAL STRESS ANALYSIS AND MATERIALS TESTING* (Vol. 601, pp. 193–196). Trans Tech Publications Ltd. <https://doi.org/10.4028/www.scientific.net/KEM.601.193>
52. Shein, E. (2015). Python for Beginners. *Commun. ACM*, 58(3), 19–21. <https://doi.org/10.1145/2716560>
53. Toth-Tascau, M., & Stoia, D. I. (2011). Analysis of dimensional accuracy of two models of customized hip prostheses made of Polyamide powder by Selective Laser Melting Technology. *Optoelectronics and Advanced Materials-Rapid Communications*, 5(12), 1356–1363.
54. van Ingen Schenau, G. J. (1984). An alternative view of the concept of utilisation of elastic energy in human movement. *Human Movement Science*, 3(4), 301–336. [https://doi.org/10.1016/0167-9457\(84\)90013-7](https://doi.org/10.1016/0167-9457(84)90013-7)
55. Vaughan, C. L., Davis, B. L., & O'Connor, J. C. (1992). *Dynamics of Human Gait*. Human Kinetics Publishers.
56. Williams, I., & Constandinou, T. G. (2014). Computationally efficient modeling of proprioceptive signals in the upper limb for prostheses: A simulation study. *FRONTIERS IN NEUROSCIENCE*, 8. <https://doi.org/10.3389/fnins.2014.00181>
57. Wu, G., van der Helm, F. C. T., Veeger, H. E. J. D., Makhsous, M., Van Roy, P., Anglin, C., Nagels, J., Karduna, A. R., McQuade, K., Wang, X., Werner, F. W., Buchholz, B., & International Society of Biomechanics. (2005). ISB recommendation on definitions of joint coordinate systems of various joints for the reporting of human joint motion--Part II: Shoulder, elbow, wrist and hand. *Journal of Biomechanics*, 38(5), 981–992. <https://doi.org/10.1016/j.jbiomech.2004.05.042>
58. Yousaf, F., Iqbal, S., Fatima, N., Kousar, T., & Shafry Mohd Rahim, M. (2023). Multi-class disease detection using deep learning and human brain medical imaging. *Biomedical Signal Processing and Control*, 85, 104875. <https://doi.org/10.1016/j.bspc.2023.104875>
59. Zajac, F. E. (1989). Muscle and tendon: Properties, models, scaling, and application to biomechanics and motor control. *Critical Reviews in Biomedical Engineering*, 17(4), 359–411.
60. Zhang, L., Li, J., Su, P., Song, Y., Dong, M., & Cao, Q. (2019). Improvement of human-machine compatibility of upper-limb rehabilitation exoskeleton using passive joints. *Robotics and Autonomous Systems*, 112, 22–31. <https://doi.org/10.1016/j.robot.2018.10.012>
61. Zhu, Z., Wang, Y., Wang, Y., & Jing, X. (2023). Nonlinear inertia and its effect within an X-shaped mechanism – Part I: Modelling & nonlinear properties. *Mechanical Systems and Signal Processing*, 200, 110590. <https://doi.org/10.1016/j.ymssp.2023.110590>
62. Zwerus, E. L., Somford, M. P., Maissan, F., Heisen, J., Eygendaal, D., & van den Bekerom, M. P. (2018). Physical examination of the elbow, what is the evidence? A systematic literature review. *British Journal of Sports Medicine*, 52(19), 1253–1260. <https://doi.org/10.1136/bjsports-2016-096712>

SCIENTIFIC ACHIEVEMENTS

Papers in WoS journals	
1.	Monica Musunoiu Novetschi , Elena Mereuta, Tarek Nazer, Daniel Ganea and Claudiu Mereuta, Human upper limb positional analysis using homogenous transformation matrix, BALNEO AND PRM RESEARCH JOURNAL, 2023;14(3):567, DOI:10.12680/balneo.2023.567, ROMANIAN ASSOC BALNEOLOGY
2.	Mereuta, E., Novetschi, M-I. , Ganea, D., Amortila, V-T., Nazer, T., (2024). Validation of the mathematical model of upper body biomechanics using neural networks, Balneo and PRM Research Journal, Accepted for publication.
3.	Mereuta, E; Novetschi, M , STUDY ON THE ENTREPRENEURIAL SKILLS OF ECONOMICAL ENGINEERING GRADUATES, MIRDEC-10TH INTERNATIONAL ACADEMIC CONFERENCE GLOBAL AND CONTEMPORARY TRENDS IN SOCIAL SCIENCES (GLOBAL MEETING OF SOCIAL SCIENCE COMMUNITY), Page41-48, 2018, https://www.webofscience.com/wos/woscc/full-record/WOS:000554404800005
Papers in SCOPUS journals	
1.	Valentin Amortilă, Elena Mereuță,, Costel Humelnicu, Mihai Gingărașu, Monica Novetschi , CONTROVERSY ABOUT CAR POLLUTION: THE ELECTRIC VEHICLE OR THE CLASSIC VEHICLE?, International Multidisciplinary Scientific GeoConference: SGEM 19 (4.2) pp. 193-200; ISBN 978-619-7408-98-0
2.	M Gingarasu, E Mereuta, V Amortila, C Humelnicu, M Novetschi , THE IMPORTANCE OF VEHICLE STEERING SYSTEM DIAGNOSIS IN REDUCING ENVIRONMENTAL IMPACT, International Multidisciplinary Scientific GeoConference: SGEM 20 (4.1), 523-530
3.	C Humelnicu, E Mereuta, V Amortila, M Gingarasu, M Novetschi , REDUCTION OF POLYMERIC WASTE BY APPLYING HEAT TREATMENTS DURING THE POLYMERIZATION PERIOD, International Multidisciplinary Scientific GeoConference: SGEM 20 (4.1), 475-481
4.	M Novetschi , E Mereuta, M Gingarasu, C Humelnicu, V Amortila THE EFFECTS OF AUTO POLLUTION ON THE POPULATION, International Multidisciplinary Scientific GeoConference: SGEM 20 (4.1), 499-506
Papers in BDI journals	
1.	C Humelnicu, V Amortila, M Novetschi , M Gingarasu, ASPECTS REFERRING TO FATIGUE TESTING OF EPOXY POLYMERIC MATERIALS, Mechanical Testing and Diagnosis 10 (3), 21-25
2.	M Gingarasu, E Mereuta, V Amortila, C Humelnicu, M Novetschi , WEAR OF SPHERICAL JOINTS OF THE VEHICLES STEERING SYSTEMS. VIBRATIONS AND THEIR ROLE IN DIAGNOSIS, Mechanical Testing and Diagnosis 10 (3), 16-20
3.	V Amortila, E Mereuta, M Novetschi , M Rus, MODELING AND SIMULATION OF THE DRIVER'S BIOMECHANICAL SYSTEM USING ADAMS SOFTWARE, Journal of Danubian Studies and Research 11 (1)
4.	V Amortila, E Mereuta, M Novetschi , M Rus, S Vereșiu, ANALYTIC MODEL OF THE SUBSYSTEM HEAD-NECK-SPINE MOVEMENT BIOMECHANICS, Mechanical Testing and Diagnosis 11 (1), 20-25
Papers in international conferences	
1	Costel Humelnicu, Valentin Amortilă, Mihai Gingărașu, Monica Novetschi , FATIGUE TESTING OF EPOXY RESIN BASED MATERIALS, Seventh Edition of the Scientific Conference of the Doctoral Schools of Dunărea de Jos” University, 13 – 14 iunie 2019, Galați, România